

**SNM NEUTRON DETECTION USING A TIME-GATED SYNTHETIC
APERTURE HYBRID APPROACH**

A Thesis
Presented to
The Academic Faculty

by

Matthew Paul Molinar

In Partial Fulfillment
of the Requirements for the Degree
Master of Science in Nuclear & Radiological Engineering in the
School of Nuclear & Radiological Engineering & Medical Physics

Georgia Institute of Technology
7/13

Copyright © M. Molinar 2013

SNM NEUTRON DETECTION USING A TIME-GATED SYNTHETIC APERTURE HYBRID APPROACH

Approved by:

Dr. Glenn E. Sjoden, Advisor
George W. Woodruff School
Georgia Institute of Technology

Dr. Chaitanya Deo
George W. Woodruff School
Georgia Institute of Technology

Dr. Chris Wang
George W. Woodruff School
Georgia Institute of Technology

Dr. Ce Yi
George W. Woodruff School
Georgia Institute of Technology

Date Approved: 05/15/ 2013

ACKNOWLEDGEMENTS

I wish to thank my Adviser and Mentor Dr. Glenn Sjoden, for the constant help, guidance, and patience he has shown me throughout my time at the Georgia Institute of Technology. I wish to thank my parents, Paul and Kathleen Molinar. Without their constant support, love, and guidance I would not be where I am today. I wish to thank my wife, Jimena, for her constant support, love, and kindness in this stressful time. Without her unyielding faith in me, I could have never accomplished this. Finally I wish to thank God, for the giving me the strength to push forward.

TABLE OF CONTENTS

	Page
ACKNOWLEDGEMENTS	iii
LIST OF TABLES	vi
LIST OF FIGURES	viii
LIST OF SYMBOLS AND ABBREVIATIONS	x
SUMMARY	xii
<u>CHAPTER</u>	
1 Introduction	1
Purpose of Research	1
Research Conducted	1
2 Model Design and Simulation Methods	3
Model Design	3
The PENTRAN Modeling	9
Initial Designs	12
Working Designs	14
The Monte Carlo (MCNP) Models	15
3 Deterministic Simulation and Verification	18
Forward Simulations	18
Adjoint Simulations	20
Convergence Investigation	21
Cadmium Free Evaluation	27
Response Coupling Procedure	28
Separate Source Simulations	31

Surface Source Simulation and Adjoint Coupling	33
4 Validation Using Adjoint Current	35
5 Source Determination	42
MCNP5 Simulation	42
Initial Spectrum Determination Using Ratio Method	49
6 Drive by Detection Simulation	54
Field of View	54
F-Factor	55
Detector Response for Traveling SNM	61
Minimum Number of Detectors	62
7 Conclusion	70
Summary of Work	70
Future Work	70
APPENDIX A-1: React Code	71
APPENDIX A-2: Areact Code	81
REFERENCES	91

LIST OF TABLES

	Page
Table 2.1: 30 Group energy structure, upper Energy value	5
Table 2.2: List of materials and their respective compositions	6
Table 2.3: List of design parameters for model designs	12
Table 3.1: Forward simulations using the initial detector design, results and simulation information	19
Table 3.2: Adjoint simulations using the initial detector design, results and simulation information	21
Table 3.3: 30 group absorption cross sections for: Cadmium, Tantalum, Hafnium, and Indium	22 - 23
Table 3.4: Cadmium free forward and Adjoint simulation	28
Table 3.5: Test model results	30
Table 3.6: Adjoint response, per source location, epithermal fission test source	32
Table 3.7: Separate Adjoint model and full Adjoint model count comparison	32
Table 3.8: Surface source and Adjoint current count comparison	33
Table 4.1: Energy detection range (MeV) for individual detector channel blocks with corresponding Adjoint importance at that energy	37
Table 5.1: MCNP5 tally responses, for various sources, and relative errors	46 - 47
Table 5.2: MCNP5 Forward response and PENTRAN model Adjoint response	48
Table 5.3: Normalized channel counts	50
Table 5.4: Channel 1 count ratios relative to Channel 3	50
Table 5.5: Channel count ratios relative to Channel 3	51
Table 5.6: Channel count ratios relative to Channel 2	52
Table 5.7: Channel count ratios relative to Channel 1	52

Table 6.1: MCNP5 tally responses for a 1.09E6 n/s PuBe source, and relative errors for 8 road side positions in simulations surrounding the center line for the vehicle	57 - 59
Table 6.2: List of F-Factor values for the MCNP5 simulations at different intervals	60
Table 6.3: R_{collided} , calculated using F-Factor compared to the R_{collided} calculated using simulation results	60
Table 6.4a: Background Emission Spectra for a Background Source Using the 47 Group Library	62 - 63
Table 6.4b: Background detector response based on a mean surface neutron flux of .02 n/cm ² /s	64
Table 6.5: Number of detectors needed for a Pu-Be source	69

LIST OF FIGURES

	Page
Figure 2.1: Multi-Channel n-detector model, with material list and dimensions	3
Figure 2.2: Absorption cross section versus energy group for 30 group library	4
Figure 2.3: 3-D model of PENTRAN detector design, half height due to bottom reflected symmetry along the z-axis	9
Figure 2.4: PENTRAN detector in Adjoint mode. Typical set up for initial simulation testing	13
Figure 2.5: Highlighted ray effect presence in simulation of design 2. Flux profile for Adjoint group 30	14
Figure 2.6: Initial detector design (left) compared to the final detector design (right)	15
Figure 2.7: MCNP5 roadside detection model, with source at 200 cm minimum (+x)	16
Figure 2.8: MCNP5 Multi-position detection simulations	17
Figure 3.1: Detector system in Forward mode	18
Figure 3.2: The initial detector design with convergence problem zones: Cadmium, Tantalum, Hafnium & Indium	20
Figure 3.3a: Absorption cross section versus 30 group structure for: Cadmium, Tantalum, Hafnium, and Indium	23
Figure 3.3b: Absorption cross section for groups 1-13 for: Cadmium, Tantalum, Hafnium, and Indium	24
Figure 3.3c: Absorption cross section for groups 1 – 7 for: Cadmium, Tantalum, Hafnium, and Indium	25
Figure 3.4: Adjoint group 1 error norm	26
Figure 3.5: Labeled detector model, with the initial detector design	26
Figure 3.6: Adjoint group 30 error norm	27
Figure 3.7: Simplified test model	30
Figure 3.8: Separate Adjoint source simulations, each Adjoint source is labeled	31

Figure 4.1: Maximum energy detection evaluation for Channels with an active Adjoint source place on Channel 1 (left-most block)	36
Figure 4.2: Maximum neutron energy to cause a detection event within a Channel for a source placed at each Channel location	38
Figure 4.3: Average neutron energy to cause a detection event within a Channel for a source placed at each Channel location	38
Figure 4.4: Adjoint importance for Channels 1-5 when the source is located at Channel 1 or 2	40
Figure 4.5: Adjoint importance for Channels 1-5 when the source is located at Channel 3, 4, or 5	40
Figure 5.1: 1 Ci Pu(WGPu) -Be Normalized source emission spectrum in the 30 group structure	43
Figure 5.2: 2.7E-03 Ci Cf Normalized source emission spectrum in the 30 group structure	44
Figure 5.3: 50 Ci Am-Be Normalized source emission spectrum in the 30 group structure	44
Figure 5.4: Surface and volumetric tally for the detector model	45
Figure 5.5: Cf-252, 14.1 MeV, Pu-Be & Am-Be Normalized source emission spectra comparison	49
Figure 6.1: Detector FOV in a road side scenario	54
Figure 6.2: Mobile SNM interval breakdown	56
Figure 6.3: Response versus SNM location in detector FOV	61
Figure 6.4: PFA and Currie limit	65

LIST OF SYMBOLS AND ABBREVIATIONS

SYMBOLS

R		Response (#/s)
Φ		Group Flux (n/cm ² /s)
σ		Cross Section (1/cm)
V		Volume (cm ³)
Φ^*		Adjoint ‘flux’
q		Source Density (n/cm ² /s)
J^\dagger		Adjoint Leakage (unitless)
A		Area (cm ²)
\bar{E}		Average Energy (MeV)
E_g		Energy Group (MeV)
S_g		# of neutrons emitted from SNM for group g (#/sec)
A_d		Detector area (cm ²)
θ		Half of the detector FoV angle
z_o		Half lane width (cm)
R_{collided}		# neutrons that collide with detector surface per time (#/s)
$R_{\text{uncollided}}$		# neutrons that do not collide with detector surface per time (#/s)
F_{factor}		Ratio of Collided to Uncollided neutrons (unitless)
σ_d		Variance in detector counts
σ_b		Variance in background counts
σ_T		Variance in SNM counts
C_b		Background count rate (#/s)

T_c	Total counting time (s)
C_L	Currie Limit (#/s)
R_T	Real activity threshold counts (#/s)
C_D	Detector count rate (#/s)
n_d	Number of detector assemblies (#)
T_R	Real counting time (s)
C_{DP}	Peak signal count (#/s)
τ	Time required for a car to pass (s)
T_p	Effective counting time (s)

ABBREVIATIONS

SNM	Special Nuclear Materials
He-3	Helium – 3
HDPE	High Density Poly-Ethylene
PENTRAN	Parallel environment neutral particle transport
TPMC	Taylor projection mesh coupling
WGPu	Weapons Grade Plutonium
Am-Be	Americium Beryllium
Cf	Californium
Pu-Be	Plutonium Beryllium
FoV	Field of View
PFA	Probability of False Alarm

SUMMARY

This work focuses on using forward and adjoint transport in a hybrid application of 3-D deterministic (PENTRAN) and Monte Carlo (MCNP5) codes to model a series of neutron detector blocks. These blocks, or “channels,” contain a unique set of moderators with 4 atm He-3 proportional detectors tuned to detect and profile a gross energy spectrum of a passing neutron (SNM) source. Ganging the units together as a large area system enables one to apply time gating the source-detector response to maximize signal to noise responses from a passing source with minimal background; multiple units may be positioned as a collective synthetic aperture detector array to be used as a way of performing real time neutron spectroscopy for detecting special nuclear materials in moving vehicles.

INTRODUCTION

1.1. Purpose of Research

With a rising need for the nations of the world to be able to actively monitor their borders for the transport of special nuclear materials (SNM), new active detection methods will be needed to maintain border security. New devices would ideally be able to detect small masses of SNM within the confines of a vehicle. A neutron based detector system should be able to (i) identify sources inside vehicles traveling at reasonable highway speeds, and (ii) perform neutron spectroscopy in order to determine the general nature of the emission spectra of the SNM being monitored.

The purpose of working towards (i) is to enable a government's border patrol to actively monitor vehicle traffic through border check points, as opposed to halting and manually inspecting every vehicle. Achieving (i) would increase the feasibility of using this system, and make incorporating this system into existing border checkpoints easier. The purpose of working towards (ii) is to enable the detector system to be able to discern between emission spectra of SNM that has been detected. This would enable the detector operator to actively determine the nature of the source – i.e. whether or not the SNM currently being detected has a thermal or a fast emission spectra. Working towards these two goals would enable governments to monitor their major borders and road ways for SNM neutron source materials.

1.2. Research Conducted

The research highlighted here focuses on designing and simulating a system that can meet the two goals presented in the previous section. This was done by utilizing a number of spectrally tuned neutron detector blocks – called “channels” – assembled in an overall system configuration to enable gross neutron spectroscopy using multiple detection channels individually designed to detect neutrons within prescribed energy ranges. Chapter 2 covers the design of these channels, and the various models used throughout the simulation portions of this research. To resolve any discrepancies arising in the early simulation portion of the work, the models underwent extensive

testing. Chapter 3 covers the testing performed on the models, tuning of the models and the detector response coupling portion of the research. This chapter goes into explicit detail on the use of Forward and Adjoint neutron transport methods in the models, and how detector response coupling was done for these two cases. Once the detector response was successfully coupled, the research moved into the next phase of testing. The modeled detector channels were individually evaluated, using the Adjoint results to determine if the individual detector channels were operating as designed. Once the accuracy of the channels were verified and the model was viewed as functional, work was performed to accomplish goals (i) & (ii). Thereafter, Chapter 5 provides an in-depth look at using the responses obtained from the individual channels in order to attempt to resolve different portions of the SNM neutron emission spectra. Chapter 6 uses the work presented in Chapter 5 to finalize the work. This chapter shows how the detector system would operate in a real life scenario, and how the system can be used to detect weak SNM in the presence of background radiation

2. MODEL DESIGN AND SIMULATION METHODS

2.1. Model Design

In pursuing this work a neutron detection model was designed that can detect neutrons with various energies that are incident on the detector surface. The detector itself consists of five separate blocks or “channels” as indicated in Figure 2.1. Each of these neutron detection channels utilizes a Helium-3 (He-3) detector array consisting of three 4 atm He-3 gas cylinders in each channel.

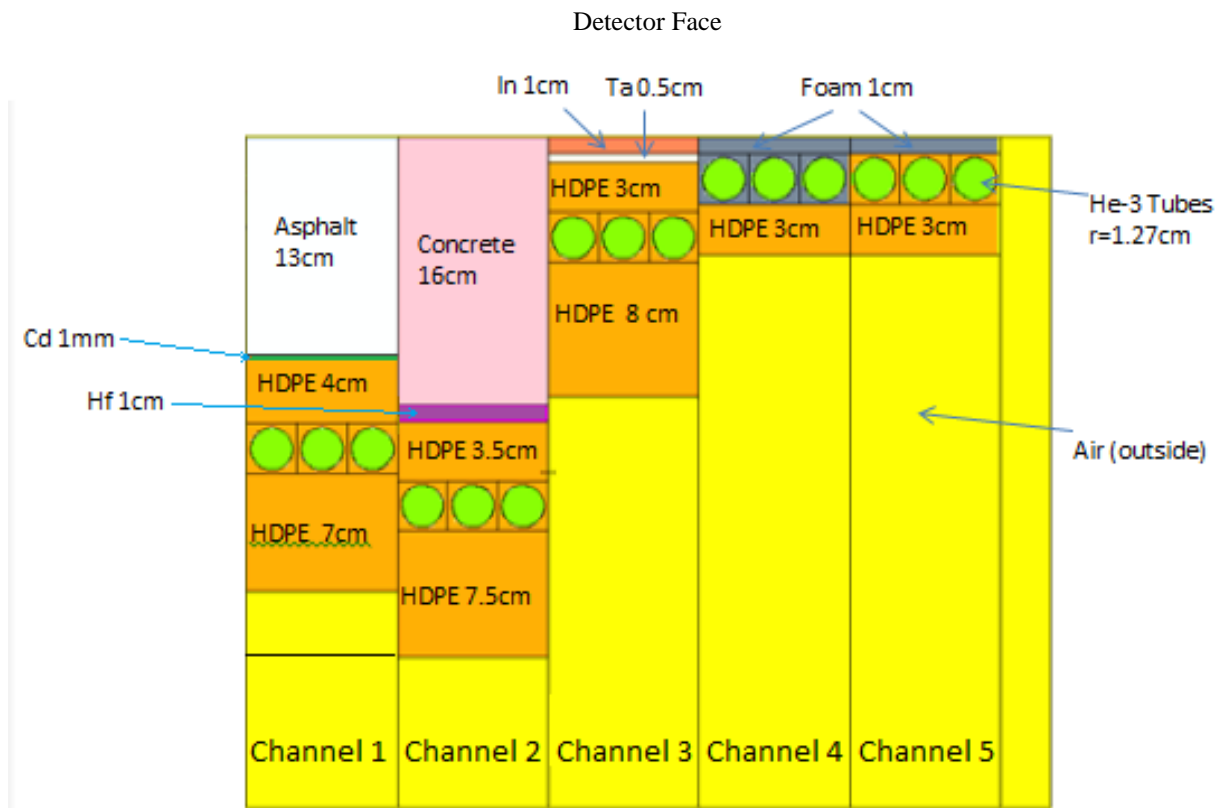
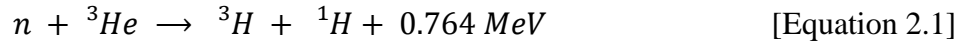


Figure 2.1: Schematic of Multi-Channel n-detector model, with material list and dimensions (cm)

Each channel is designed based on transport analysis to detect incident neutrons within a specific energy range, and register the subsequent counts within the pressurized He-3 tubes via an (n,p) reaction shown below in Equation 2.1 [1].



The reaction works by reacting a neutron with a He-3 nucleus resulting in a Tritium (${}^3\text{H}$) nuclide and a proton (${}^1\text{H}$) [1]. While neutrons of nearly any incident energy will cause the reaction to occur, the absorption cross section is weak in the fast neutron energy range, and very strong in the thermal neutron energy range, as seen in Figure 2.2 [2].

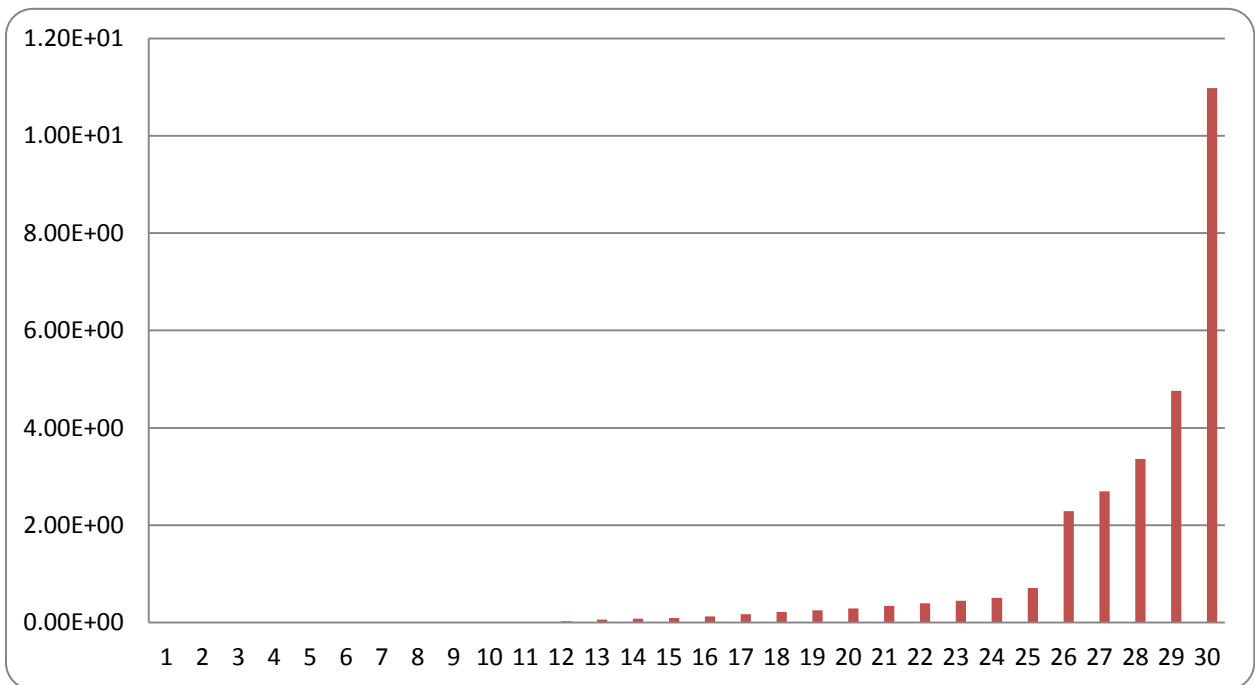


Figure 2.2: Absorption cross section versus energy group for 30 group library.

Figure 2.2 shows the absorption cross section for the He-3 detector's that were used in the simulation versus a 30 group library (determined independently from an adjoint weighted group collapse) used for the deterministic simulations in PENTRAN and MCNP. The group structure used is shown below in Table 2.1.

Table 2.1: 30 Group energy structure, upper Energy value

Grp #	E (MeV)
1	18.6665
2	12.76015
3	5.59365
4	2.25
5	1.375
6	1
7	0.51
8	0.1575
9	0.029
10	0.007275
11	0.000794
12	2E-05
13	2.18E-06
14	1.15E-06
15	8.13E-07
16	4.88E-07
17	2.63E-07
18	1.5E-07
19	1.13E-07
20	8.5E-08
21	6E-08
22	4.5E-08
23	3.5E-08
24	2.77E-08
25	1.34E-08
26	1.35E-09
27	9.75E-10
28	6.25E-10
29	3E-10
30	5E-11

Table 2.1, in conjunction with Figure 2.2, shows that as the energy of an incident neutron decreases into the eV range, the absorption cross section for the He-3 detectors increases – increasing the probability of the reaction highlighted in Equation 2.1 taking place. Therefore, fast neutrons must first be moderated down into the thermal energy range to be detected; this is accomplished by utilizing various moderator materials. Material specifications, and compositions needed in this work are provided in Table 2.2 below. These materials in each detector channel were optimized by transport computations in a unique configuration to act as a “selective neutron energy filtration system”, as detailed below:

Table 2.2: List of materials and their respective compositions

Material	Density (g/cm ³)	Material Fractions
Asphalt	2.376	H-1: -10.19, C-12: -85.78, N-14: -.26, S-32: -3.41, O-16: -.36, V-46: -7E-04, Ni-58: -4E-05
Cadmium	8.65	Cd: 1.0
Concrete	2.3	H-1: 1.3741E-02, Si-28: 1.662E-02, O-16: 4.6056E-02, Al-27: 1.7454E-03, Na-23: 1.7472E-03, Ca-40: 1.5206, Fe-54: 2.0139E-05, Fe-56: 3.1847E-04, Fe-57: 2.6393E-06, Fe-58: 9.7068E-07
Dow Foam	3.5E-02	H-1: 3.0053E-03, C-12: 1.5026E-03
Hafnium	13.31	Hf: 1.0
High Density – Polyethylene	.95	H-1: 8.171E-02, H-2: 9.399E-06, C-12: 4.077E-02
Indium	7.3	In: 1.0
Tantalum	16.69	Ta: 1.0

** “-” indicates a weight fraction

- *Channel 1:* Designed to filter out incident neutrons with low energies, and detect fast neutrons with energies in excess of 3.68 MeV [3]. This energy cutoff was determined using Adjoint transport simulations of the block to find the lowest energy neutron that would cause an event. Neutrons first encounter a 13 cm block of asphalt. This block provides scatter and absorption of incident thermal neutrons; in addition, it also provides down-scatter moderation for fast neutrons. A thin strip of cadmium is layered after the asphalt block. This cadmium strip acts as a neutron filter for epithermal and thermal neutrons by absorbing them. The cadmium strip also provides additional moderation of fast neutrons, by down scattering these neutrons as they pass through. After the cadmium

strip is a block of high density polyethylene (HDPE) that serves as an additional moderator, without having the same extreme absorption cross section as the previous cadmium strip. This allows for neutrons to experience additional down scatter, while allowing them to pass through the HDPE toward the detector. The final layer of material was the He-3 tubes, surrounded by HDPE. This was done to provide any final moderation for epithermal neutrons. Any thermal neutrons that are incident on the He-3 tubes will be registered as neutrons counts. Behind the He-3 detector is a HDPE reflector to reflect neutrons not absorbed in the He-3 tubes back into these detectors. The full block is 9cm wide (X), by 27 cm long (Y), by 30 cm deep (Z).

- *Channel 2:* Designed to detect incident fast neutrons within the energy range of 1.0 to 3.68 MeV [3]. The incident neutrons will first come in contact with a concrete block. This block provides scatter of incident fast neutrons, while scattering and absorbing any incident thermal neutrons. This block is followed by a strip of Hafnium, this strip acts like a neutron filter. The strip provides moderation for fast neutrons via scattering, while also scattering and absorbing any epithermal or thermal neutrons. This strip is followed by a block of HDPE. This block provides additional moderation for any remaining fast neutrons. The moderated fast neutrons will then be incident to the He-3 detectors surrounded by HDPE. This will provide any final moderation that is needed, while ensuring that the neutrons are detected. Behind the He-3 detector is a large sheet of HDPE reflector, to reflect neutrons that were not initially absorbed into the He-3 back into the detectors. The full block is 9cm wide (X), by 31 cm long (Y), by 30 cm deep (Z).
- *Channel 3:* Designed to detect low energy fast neutrons within the energy range of 0.369 to 1.0 MeV [3]. This is accomplished by layering 1.0 cm of Indium and 0.5 cm thick Tantalum sheets in succession. The Indium sheet allows fast neutrons to be scattered, and pass through, while absorbing and epithermal or thermal neutrons that are incident on the surface. The Tantalum sheet allows mid to low energy fast neutrons to stream through and provides moderation for these particles. The sheet also acts as an absorber for any thermal neutrons that passed through the Indium sheet. The scattering provided by the dual sheets of Indium and Tantalum will moderate the low energy fast neutrons into the

epithermal/thermal range. The neutrons will then enter the He-3 detectors surrounded by HDPE. The HDPE will help provide the additional moderation needed to bring neutrons into the thermal detectable range. The neutrons that enter into the He-3 detector at this point will be register as a count. Thermal neutrons that were not detected are reflected back into the He-3 tubes by a HDPE layer behind the detector. This layer will also act as an additional moderator and absorber for any high energy fast neutrons that entered into this channel, but not designed to be detected by this channel. The full block is 9cm wide (X), by 15.5 cm long (Y), by 30 cm deep (Z).

- *Channel 4:* Designed to detect incident neutrons with an average energy of approximately 1keV. The first layer of material in this channel is a sheet of low density foam (Dow foam). This foam will allow epithermal neutrons to stream through, and provide moderation for these neutrons. The next layer is the He-3 detectors surrounded by additional Dow foam. The additional foam provides any final moderation that is needed to allow for the detectors to register the neutrons. Any thermal neutrons that were not initially detected by the He-3 detectors will then be reflected by the sheet of HDPE behind the array. This sheet will also scatter and absorb any moderate energy neutrons that entered into this channel. The full block is 9cm wide (X), by 7 cm long (Y), by 30 cm deep (Z).
- *Channel 5:* Designed to detect incident neutrons with an average energy of approximately 700 eV. This is done by limiting the amount of absorption that can possibly take place in this channel. To accomplish this, a layer of HDPE is used for any moderation that would be need. The next layer consists of He-3 surrounded by HDPE, which will provide any final moderation that is needed. The thermal neutrons will then register as count within the detectors, and any thermal neutrons that were not registered as counts initially will be reflected by a sheet of HDPE behind the detectors. The full block is 9cm wide (X), by 7 cm long (Y), by 30 cm deep (Z).

In order to have the freedom to place the assembled detector channel modules in a number of arbitrary remote monitoring locations for integrated assessment purposes, the application of Adjoint computations will facilitate obtaining a response in each channel for “arbitrary

placement” by coupling the arriving radiation current with the Adjoint current on the front faces of the detectors to render a response. Therefore, the multichannel detector model was constructed in both PENTRAN (Parallel Environment Neutral-particle TRANsport) for 3-D deterministic calculations and in MCNP5 for Monte Carlo based simulations, respectively.

2.2. The PENTRAN Modeling

The PENTRAN model based on Figure 2.1 was initially designed using the PENMSHXP code mesh generator system. This system allowed for design of the detector system in a 3-D environment, and a detailed version of the final model is shown below in Figure 2.3 detailed image generation.

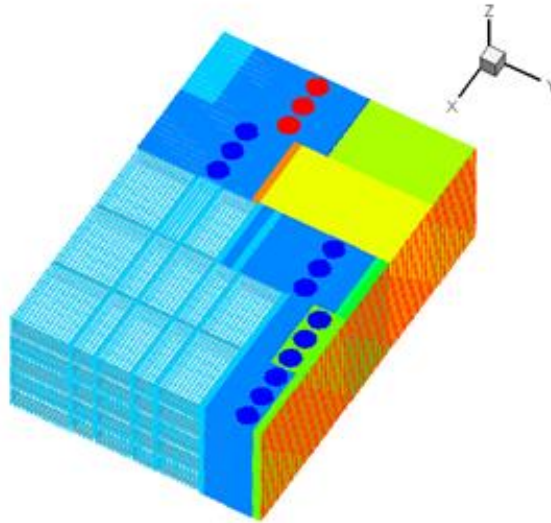


Figure 2.3: 3-D model of PENTRAN detector design, half height due to bottom reflected symmetry along the Z-axis.

The deterministic simulations were then performed using the PENTRAN parallel Sn code system [4]. This code is used for 3-D multigroup Forward and Adjoint discrete ordinate transport simulations; the code is optimized for parallel computing, and can solve problems by decomposing the problem variables over angle, energy group, and space, allowing for hyper-accurate neutron transport simulations on a fine mesh basis. The accuracy and versatility of this

program supported by 3-D mesh generation tools allows for multigroup transport solutions to be rendered for complex detector systems [5].

PENTRAN operates by iteratively solving the transport equation, shown below as Equation 2.1 [5].

$$\begin{aligned} \widehat{\Omega} \cdot \vec{\nabla} \psi(\vec{r}, E, \widehat{\Omega}) + \sigma(\vec{r}, E) \psi(\vec{r}, E, \widehat{\Omega}) &= q^{\text{ext}}(\vec{r}, E, \widehat{\Omega}) \\ + \int_0^\infty dE' \int d\widehat{\Omega}' \sigma_s(\vec{r}, E' \rightarrow E, \widehat{\Omega} \cdot \widehat{\Omega}') \psi(\vec{r}, E', \widehat{\Omega}') \\ + \frac{\chi(\vec{r}, E)}{k} \int_0^\infty dE' \int d\widehat{\Omega}' \nu \sigma_f(\vec{r}, E') \psi(\vec{r}, E', \widehat{\Omega}') \end{aligned} \quad [\text{Equation 2.1}]$$

Where,

- $\widehat{\Omega}$ is the solid angle in the direction of motion
- $\psi(\vec{r}, E, \widehat{\Omega})$ is the angular neutron flux, about \vec{r} , with energy E , and moving about $\widehat{\Omega}$
- $\sigma(\vec{r}, E)$ is the total cross section for all reactions
- $q^{\text{ext}}(\vec{r}, E, \widehat{\Omega})$ is the external source
- $\sigma_s(\vec{r}, E' \rightarrow E, \widehat{\Omega} \cdot \widehat{\Omega}')$ is the scattering cross section from initial energy E' to final energy E moving about initial direction $\widehat{\Omega}'$ into final direction $\widehat{\Omega}$
- $\chi(\vec{r}, E)$ is the probability density function for neutrons produced by all fission
- k is the neutron balance for the system of neutrons produced over neutrons lost
- $\nu \sigma_f$ is the neutrons produced by fission interactions

For a fixed source problem, Equation 2.1 can be written for Forward and Adjoint transport as Equations 2.2 and 2.3 respectively [5].

$$H\psi_g = q_g \quad [\text{Equation 2.2}]$$

$$H^\dagger \psi_g^\dagger = \sigma_{dg} \quad [\text{Equation 2.3}]$$

Where H and H^\dagger are the Forward and Adjoint multigroup transport operators, given below in Equations 2.4 and 2.5 respectively [5]. ψ_g is the forward angular flux [$\#/\text{cm}^2/\text{s}/\text{sr}$] and q_g is

the fixed source magnitude [#/cm²/s/sr] [5]. ψ_g^\dagger is the Adjoint expected counts per particle [unitless] and σ_{dg} is the detector absorption cross section [cm²] [5].

$$H = \hat{\Omega} \cdot \nabla + \sigma_g(\vec{r}) - \sum_{g'=1}^G \int_{4\pi} \sigma_{s,g' \rightarrow g}(\vec{r}, \hat{\Omega}' \cdot \hat{\Omega}) d\hat{\Omega}' \quad [\text{Equation 2.4}]$$

$$H^\dagger = -\hat{\Omega} \cdot \nabla + \sigma_g(\vec{r}) - \sum_{g'=1}^G \int_{4\pi} \sigma_{s,g \rightarrow g'}(\vec{r}, \hat{\Omega} \cdot \hat{\Omega}') d\hat{\Omega}' \quad [\text{Equation 2.5}]$$

Where the Adjoint operator reverses the direction of streaming, and inverts the scattering group-to-group energy coupling and the directional terms. Applying the principle of reciprocity through inverting the relationship between the source and detector leads to the relationship between Forward and Adjoint shown in Equation 2.6.

$$\langle \psi^\dagger H \psi \rangle = \langle \psi H^\dagger \psi^\dagger \rangle \quad [\text{Equation 2.6}]$$

Substituting Equation 2.4 and 2.5 into 2.6, the Reaction Rate Equivalency between Forward and Adjoint reaction rates is found, shown in Equation 2.7.

$$R = \langle \psi_g \sigma_{dg} \rangle = \langle \psi_g^\dagger q_g \rangle \quad [\text{Equation 2.7}]$$

Taking a volumetric basis, reaction rates can be found for the Forward and Adjoint detection reactions, as shown below in Equation 2.8 and 2.9 respectively.

$$R_{fwd} = \langle \Phi \sigma_d \Delta V_d \rangle \quad [\text{Equation 2.8}]$$

$$R_{adj} = \langle \Phi^\dagger q_{fwd} \Delta V_s \rangle \quad [\text{Equation 2.9}]$$

Where, Φ is the scalar flux, attained by integrating over all angles [n/cm²/s], σ_d is the isotropic absorption cross section for the detector [cm²], and ΔV_d is the detector volume [cm³]. Φ^\dagger is the scalar adjoint importance [unitless], q_{fwd} is the volumetric forward source [# /cm³/s],

and ΔV_s is the source volume [cm³]. Equation 2.9 can be recast with an area basis to obtain the response using Adjoint currents; the result of this is shown in Equation 2.10.

$$R_{adj} = \langle J^\dagger q_{fwd}^- \Delta A_s \rangle \quad [\text{Equation 2.10}]$$

Where, J^\dagger is the adjoint current [unitless], q_{fwd}^- is the forward source current projected towards the detector face [#/cm²/s], and ΔA_s is the area of the detector face [cm²]. The PENTRAN code system can be used to generate the J^\dagger term for Equation 2.10, and the Φ term for Equation 2.8. It is for this reason that the PENTRAN code system will be used for Forward and Adjoint simulations in this work.

2.3. Initial Designs

The initial design phase of this work showcases the progression through the first three ‘approximate’ designs. The breakdown of these designs covers the circumstances under each testing, and the changes that were made in order to attain a reliable model. The design parameters for each of the model configurations are listed under Table 2.3 below.

Table 2.3: List of design parameters for model designs

Design	SN	Total Coarse Mesh	Total Fine Mesh	Total Z
1	4	30	611,010	1
2	6	200	621,810	5
3	12	200	1,385,280	5
4 – initial detector design	10	200	1,249,560	5
5 – final detector design	10	250	1,020,240	5

This table categorizes the various model designs and meshing configurations that were evaluated in the simulations. Each simulation was subjected to an identical test: simulate an Adjoint run with a S₄ level symmetric quadrature. For the Adjoint simulation, the Adjoint source meshes were the 4 atm pressurized He-3 detector tubes – as shown in Figure 2.3 – with an energy spectrum that was the absorption cross sections for He-3 with an Adjoint group

configuration ($E_1 = E_{30}$). The error tolerance was evaluated in the target meshes, the “air strip” mesh regions located at the top of the model – also highlighted in Figure 2.4.

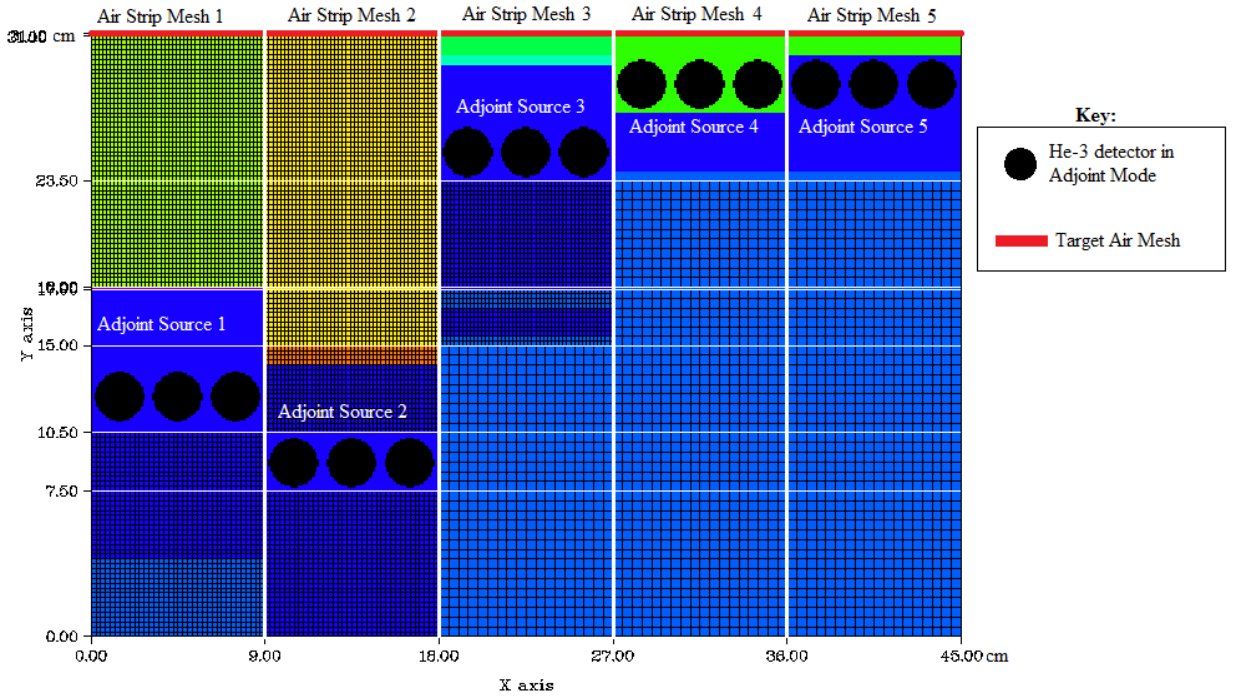


Figure 2.4: PENTRAN detector in Adjoint mode. Typical set up for the benchmark simulation testing.

In order for a model to be satisfactory, it had to achieve flux convergence with an error tolerance of $<1.0E-03$. Using this requirement, Designs 1, 2, and 3 were simulated using the PENTRAN code system. The results of these simulations were evaluated, and are presented in Table 2.3. In Design 1, it was determined that the design was specified with too few coarse meshes. To correct for the lack of coarse and requisite fine meshing, ten additional coarse meshes were added in the x and y dimensions of the model, and an additional 10,800 fine meshes were added to the model. The total depth the model (Z -axis) was then split up into 5 identical levels, with a reflective boundary condition along the bottom of the model. Design 2 was simulated, and it was determined that the design was inadequate due to some ray effects noted in some energies in the results. An example displaying some minor ray effects is shown in Figure 2.5 below. The ray effects presence is attributed to an under sampling in angular flux vectors. To correct for the error that ray effects introduce, Design 2 was remeshed – increasing the number

of fine meshes from 621,810 to 1,385,280, and modifying the angular quadratures to an order that enabled better representation of the particle transport phase space.

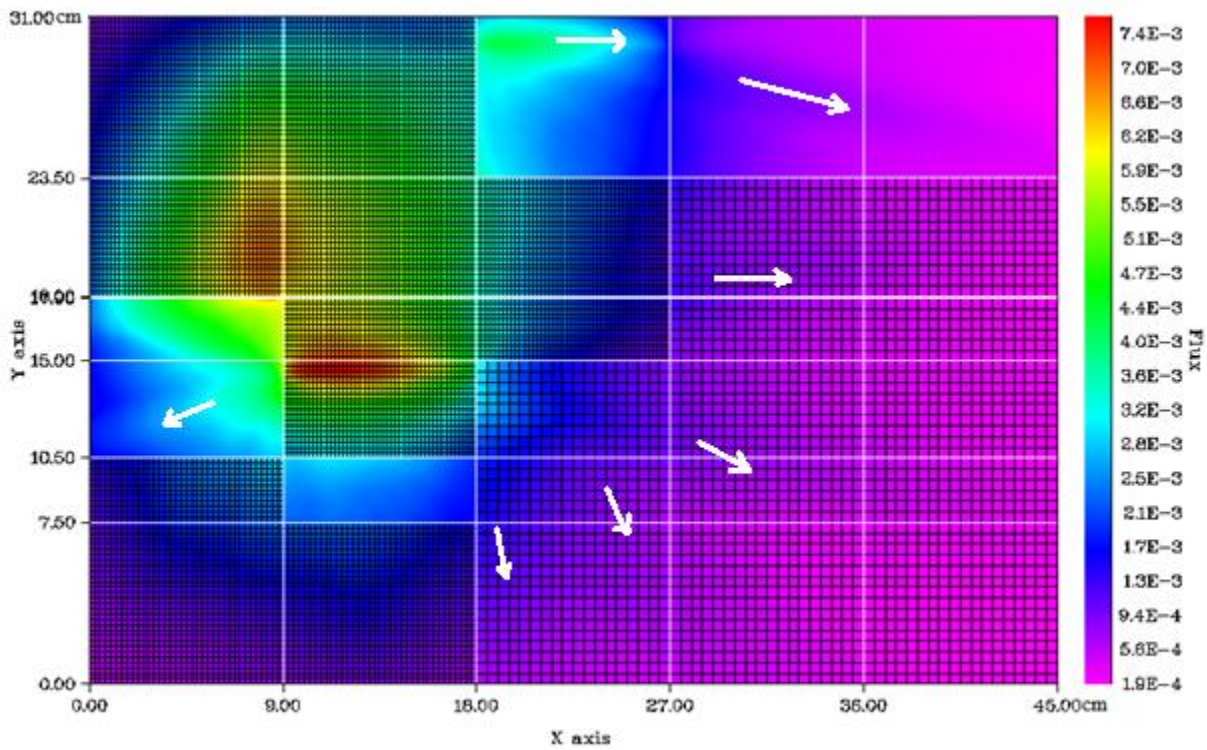


Figure 2.5: Highlighted ray effect presence in simulation of design 2 with a 3-D level symmetric quadrature of 6. Flux profile for Adjoint group 30. $E = 18.665$ MeV.

Design 3 was evaluated, and it was determined that the design was approaching its maximum run time due to an imbalance arising from the Taylor Projection Mesh Coupling (TPMC) in PENTRAN [5]. It was rectified by keeping the ratio of fine meshes at common coarse mesh boundaries to a 1:4 minimum.

2.4. Working Designs

Design 4 was simulated, and it achieved the required convergence of $< 1 \text{ E-}03$ as an infinity norm among target meshes. This model was used for the initial phases of the research. However, as the testing progressed, a discrepancy arose in the data that was traced back to a minor meshing flaw in this design. Design 5 – the final detector design – saw an addition of an extra level of coarse meshes, and an increase in the fine meshing for the Cadmium material zone. Figure 2.6

shows a comparison of these two designs. This new design added two additional coarse meshes in the y direction, and reduced unnecessary fine meshing, while increasing fine mesh density in the cadmium material zones. The new design retained the proper convergence in the target meshes, while minimizing computer execution time.

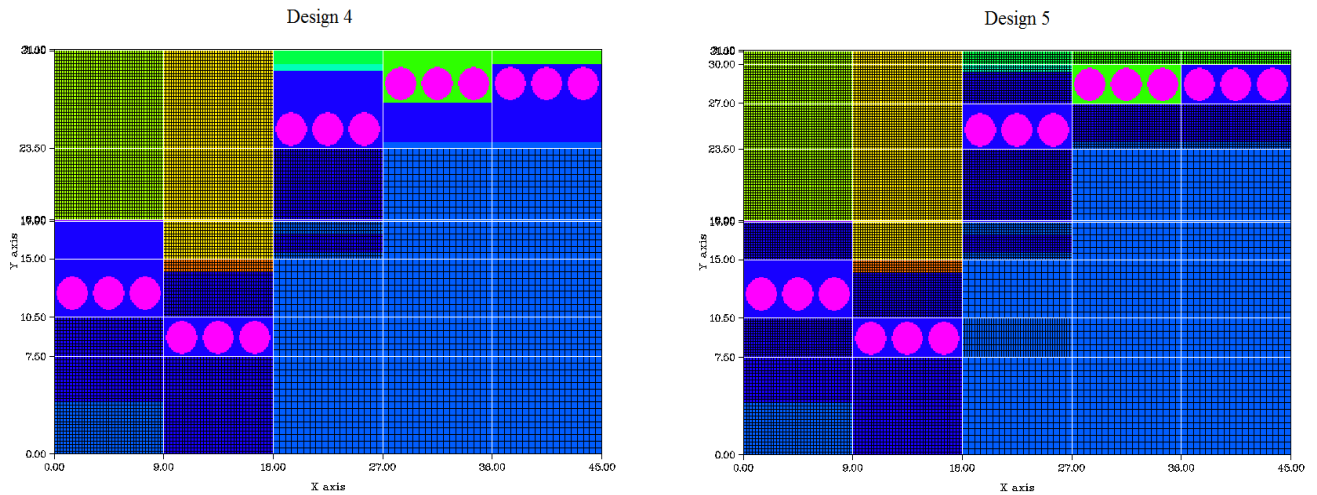
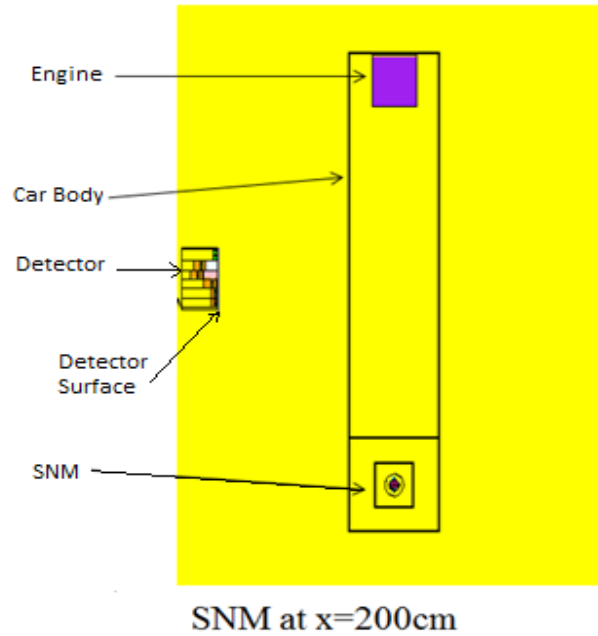


Figure 2.6: Initial detector design (left) compared to the final detector design (right).

2.5. The Monte Carlo (MCNP) Models

Monte Carlo computations were accomplished via the standard MCNP5 code system developed at Los Alamos National Laboratory [6]. Monte Carlo based simulation was used for this work as an independent method in which to model the actual geometry of the system. MCNP5 also uses simulations with a continuous energy system – as opposed to PENTRAN, which uses discretized “multigroup” energy cross sections from the 30 group library (as discussed). A Monte Carlo model was developed to simulate a roadside environment, and based on previous investigations of “typical” automobiles and roadways in the United States, a region of interest spanning +/- 200 cm as a “Field of View”, along with a 200 cm range to the SNM target placed in an automobile. The details of the 200 cm field of view will be in section 6.1. The MCNP5 model was constructed as an all-inclusive model, featuring the roadbed, a roadside multichannel detector model assembly, and an SNM mass located in the trunk of a passing vehicle, as presented in Figure 2.7. This model is designed to determine multi-channel detector

response in a realistic scenario, and to generate a planar source term to be used later to couple with the multi-channel Adjoint current obtained from the PENTRAN deterministic simulator.



**Figure 2.7: MCNP5 roadside detection model, with source at 200 cm minimum (+x).
Steel car body on asphalt road surface with full gas tank (octane) [2]**

No multiple meshing simulations were required for this phase of the work; however, several variations of this model were used. Figure 2.8 illustrates an example of what these model variations were.

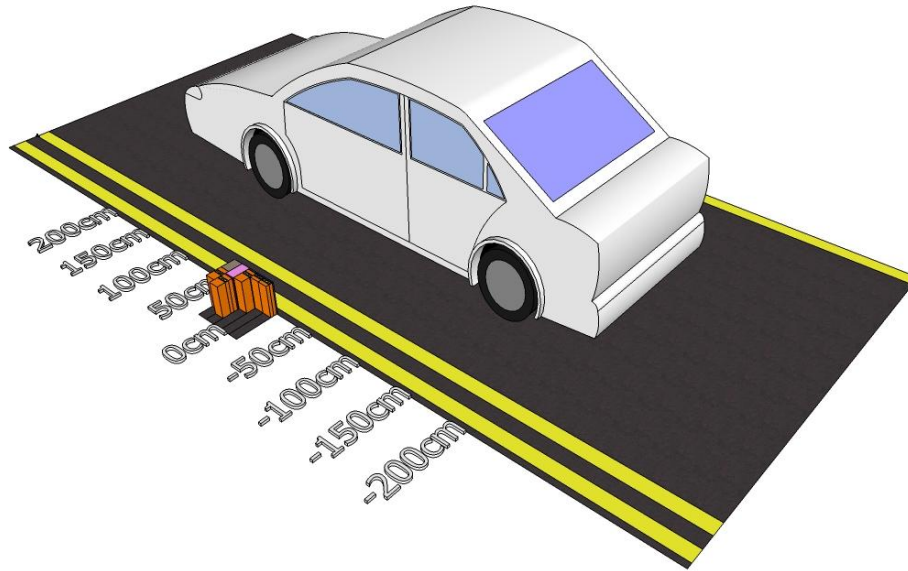


Figure 2.8: MCNP5 Multi-position detection simulations.

The model variations investigated had the detector being shifted to different positions – marked as: ± 50 , ± 100 , ± 150 , and ± 200 cm in Figure 2.8 – along the road side to simulate the detector response for a car as it drives by the source.

3. DETERMINISTIC SIMULATION AND VERIFICATION

3.1. Forward Simulations

This section of the research covers the Forward simulations performed in the PENTRAN code system using the initial detector design. The subsequent section covers the Adjoint simulations that were simultaneously performed. Figure 3.1 shows the setup of a typical Forward simulation in PENTRAN.

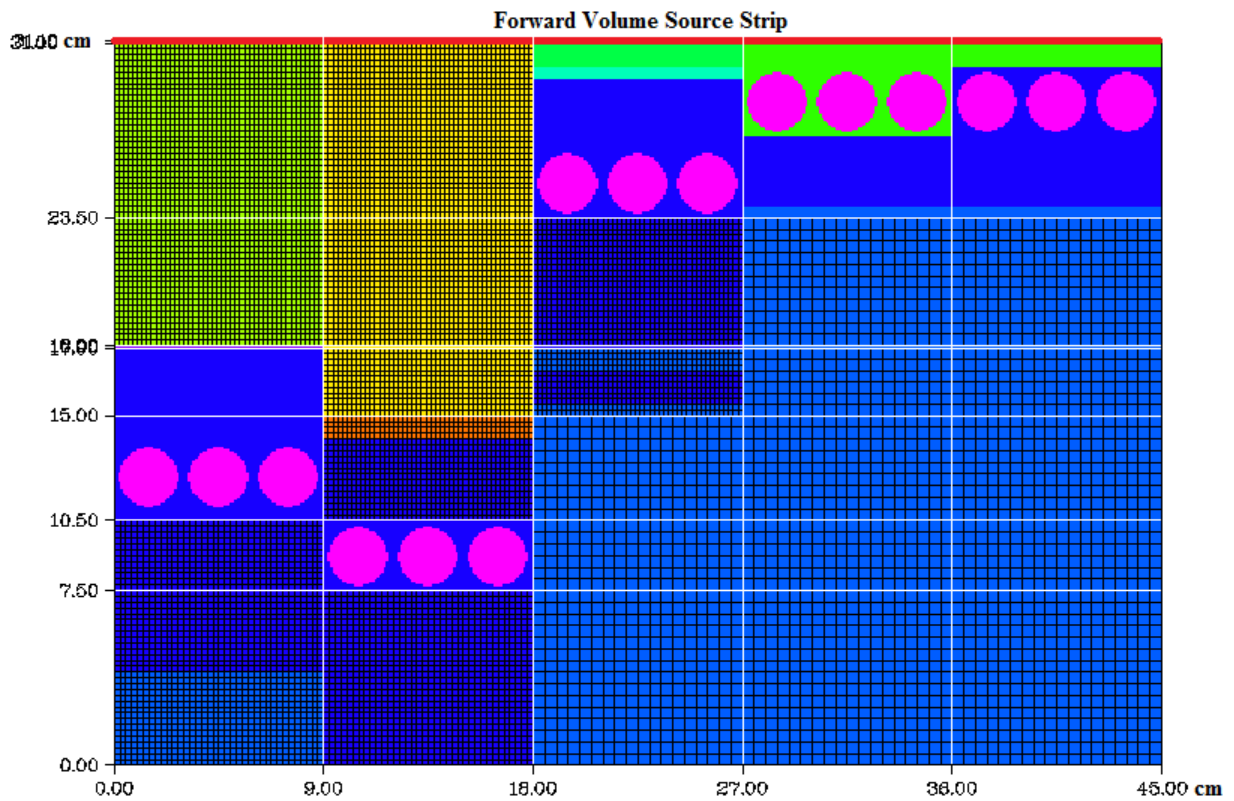


Figure 3.1: Detector system in Forward mode.

The source strip – located along the top of the model as seen in Figure 3.1 – was a 30 group source spectrum (optimized from the Bugle-96 47 group library [2]) for an epithermal fission test source.

Using this set up, three separate simulations were performed in succession. The primary difference between the simulations was an increase in the 3-D level symmetric quadrature from

S₄ to S₆ to S₁₂. Each of these simulations was performed with P₂ scattering computation and a flux convergence tolerance of 1.0E-03. However, the convergence that was tested for this portion of the simulations differed from the model design test. For these simulations (both Forward and Adjoint) convergence is being upheld globally, not just in specific target meshes – which were the He-3 detectors. The results for these 3 Forward simulations are presented in Table 3.1.

Table 3.1: Forward simulations using the initial detector design, results and simulation information

Run	Iterations	Sn	Results Converged	Infinity Norm (global) Convergence Achieved	Ray Effect
1	80	4	N	1.50E-02	Y
2	80	6	N	2.40E-02	N
3	80	12	N	2.60E-02	N

Because of the simulations convergence problems, the results of the final Forward simulation were evaluated on a coarse ‘mesh-by-mesh’ case. This method involved going into the output files and extracting the final convergence error in each of the coarse meshes, and evaluating which coarse meshes/material zones had the greatest localized error. With this method it was found that the majority of the convergence issues stemmed from the mesh regions containing strongly absorbing materials, including Cadmium, Tantalum, Hafnium, and Indium. Figure 3.2 highlights the convergence zones where local convergence difficulty was noted. This kind of inconsistency can be corrected by greatly increasing the number of fine meshes in the appropriate material zones.

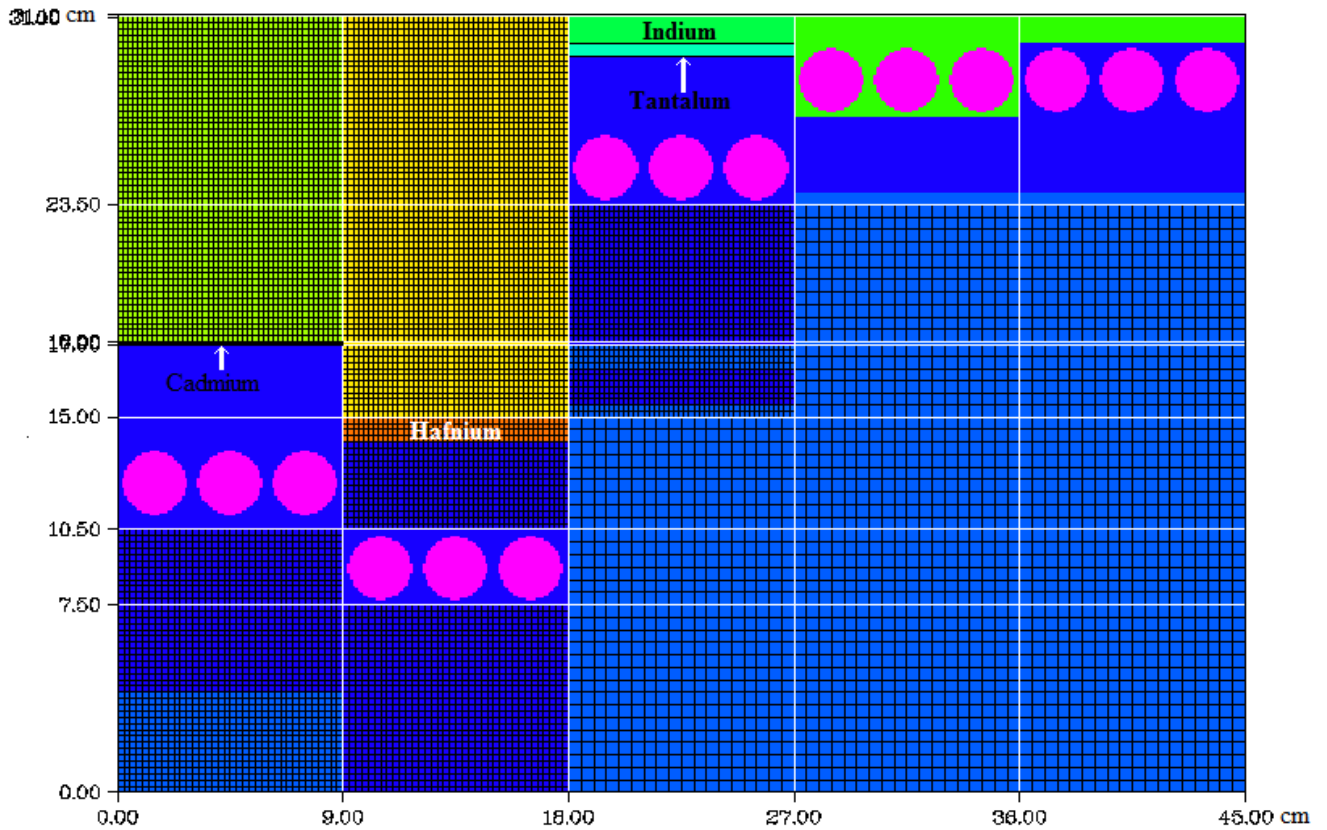


**Figure 3.2: The initial detector design with convergence problem zones: Cadmium
Tantalum, Hafnium & Indium.**

3.2. Adjoint Simulations

The Adjoint simulations for this work were performed using the initial detector design, and were executed simultaneously with the Forward simulations. As discussed, in the way it is applied here, the adjoint function is essentially detector efficiency. The sources for the Adjoint simulations were located in the He-3 detector tubes, as shown previously in Figure 2.3, with an energy spectrum of the absorption cross sections for He-3 aliased as the adjoint source [8]. The group structure used the same 30 group reference library with an Adjoint group configuration ($E_{1,\text{fwd}} = E_{30,\text{adj}}$).

For the Adjoint simulations performed on the initial detector design, three separate cases were run. Each case had an increase in the level symmetric quadrature from S_4 to S_6 to S_{12} . Each

of the three simulations that were performed utilized P_2 scattering computation and had a flux convergence tolerance of $1.E-3$. The results of these three simulations can be seen in Table 3.2 below.

Table 3.2: Adjoint simulations using the initial detector design, results and simulation information

Run	Iterations	Sn	Pre Flx Made	Pre Flx Used	Results Converged	Convergence Achieved	Ray Effect
1	80	4	Y	N	N	1.67E-02	Y
2	80	6	Y	Y	N	2.47E-02	N
3	80	12	Y	Y	N	2.72E-02	N

The final Adjoint and Forward simulations were evaluated at approximately the same time, and a similar ‘mesh-by-mesh’ evaluation was performed for the final Adjoint simulation. The findings of this coarse mesh convergence analysis were synonymous with the findings from the Forward analysis: the convergence issues in the simulation were being driven by the four material zones: Cadmium, Tantalum, Hafnium, and Indium.

3.3. Convergence Investigation

In our efforts to compose Adjoint transport models for arbitrary placement of the detector array modules for the system design, a highly converged Adjoint model is required. In doing so, we note that the detector design developed for this project utilizes several unique materials that are problematic when attempting to achieve iterative solution convergence these material zones, and the materials are: cadmium, tantalum, hafnium, and indium. The principal cause of model convergence challenges are related to the material respective absorption cross sections of these materials [4]. The 30 group materials absorption cross sections can be noted in Table 3.4, they are also graphically represented in Figures 3.3a, 3.3b, and 3.3c. Observing the cross sections for cadmium, it can be seen that as the energies decrease, the cross section for absorption dramatically increases. This creates a localized problem zone in the transport sweep over the phase space that acts like a filter due to low energy resonance for neutrons in energy groups greater than group 18. Even with exponential differencing schemes in adaptive differencing 3-D

deterministic models, the relative iterative error in the zone cannot be resolved below 1.0E-03 with the models current configuration, and as a result this zone will cause convergence problems for neutrons that are being absorbed in the zone and not passing through the ‘filter’.

Table 3.3: 30 group absorption cross sections for: Cadmium, Tantalum, Hafnium, and Indium

Group	Cadmium [cm^{-1}]	Tantalum [cm^{-1}]	Hafnium [cm^{-1}]	Indium [cm^{-1}]
1	1.41E-03	5.99E-04	1.13E-03	7.58E-04
2	8.78E-04	4.55E-04	6.83E-04	4.73E-04
3	4.47E-04	7.65E-04	1.08E-03	9.14E-04
4	1.16E-03	2.91E-03	2.41E-03	5.59E-03
5	1.92E-03	5.58E-03	4.14E-03	8.66E-03
6	2.81E-03	7.14E-03	4.61E-03	9.21E-03
7	4.45E-03	1.09E-02	6.00E-03	9.41E-03
8	7.35E-03	1.71E-02	1.12E-02	1.37E-02
9	1.99E-02	5.12E-02	2.66E-02	3.60E-02
10	5.25E-02	1.54E-01	6.99E-02	6.50E-02
11	4.32E-02	3.02E-01	3.21E-01	6.23E-02
12	2.02E-02	6.82E-01	6.23E-01	2.39E-01
13	1.76E-01	4.53E-01	3.87E+00	1.57E+00
14	4.17E-01	2.62E-01	2.45E+01	1.55E+01
15	2.19E+00	2.70E-01	4.07E+00	5.82E+00
16	5.79E+00	3.11E-01	2.12E+00	3.71E+00
17	4.03E+01	3.86E-01	1.93E+00	3.32E+00
18	2.95E+02	4.95E-01	2.19E+00	3.64E+00
19	1.90E+02	5.72E-01	2.45E+00	4.01E+00
20	1.40E+02	6.55E-01	2.75E+00	4.45E+00
21	1.16E+02	7.71E-01	3.18E+00	5.10E+00
22	1.09E+02	8.83E-01	3.60E+00	5.74E+00
23	1.09E+02	9.98E-01	4.04E+00	6.43E+00
24	1.12E+02	1.12E+00	4.51E+00	7.14E+00
25	1.28E+02	1.56E+00	6.12E+00	9.35E+00

Table 3.3 Continued

26	3.79E+02	5.02E+00	1.99E+01	3.11E+01
27	4.37E+02	5.73E+00	2.25E+01	3.52E+01
28	5.52E+02	7.35E+00	2.91E+01	4.57E+01
29	7.56E+02	1.01E+01	4.06E+01	6.47E+01
30	1.71E+03	2.30E+01	9.28E+01	1.49E+02

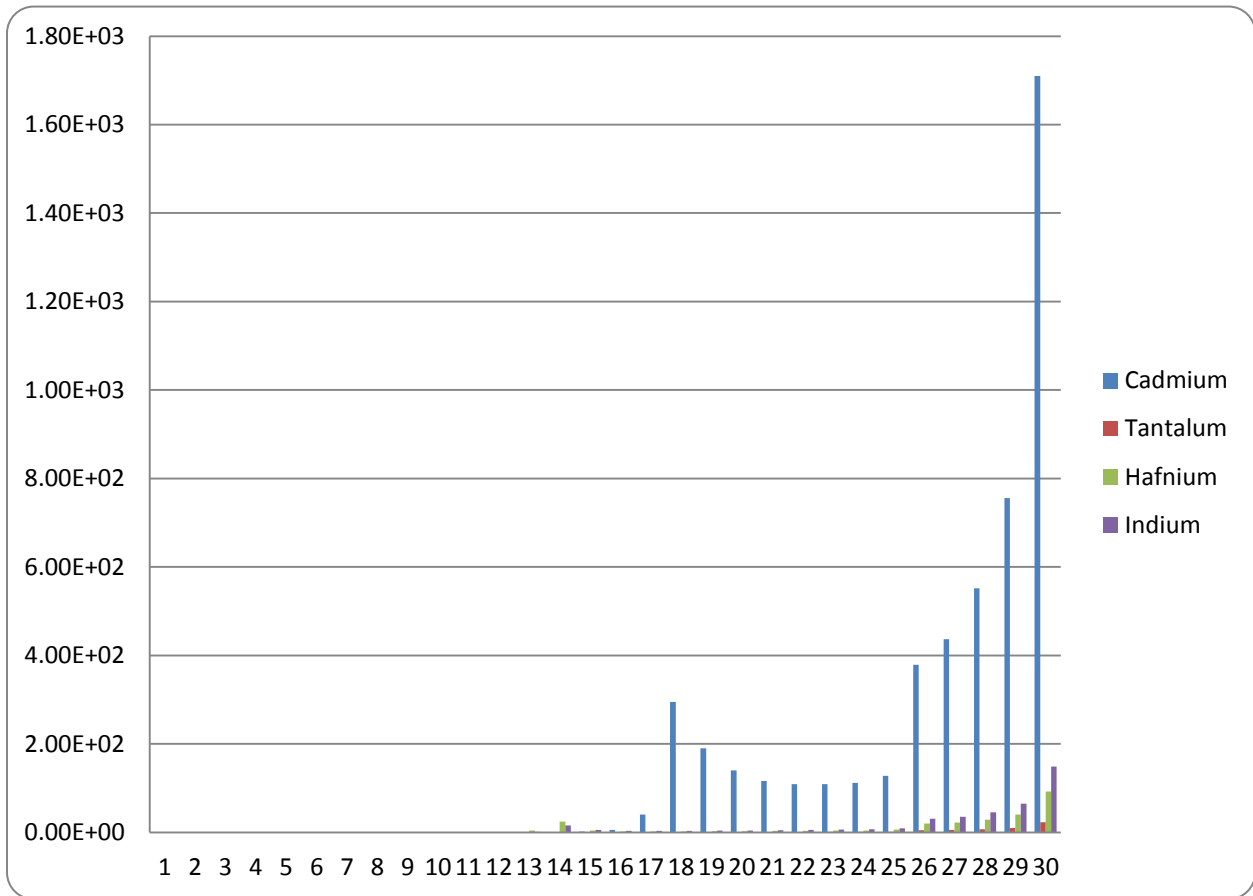


Figure 3.3a: Absorption cross section versus 30 group structure for: Cadmium, Tantalum, Hafnium, and Indium

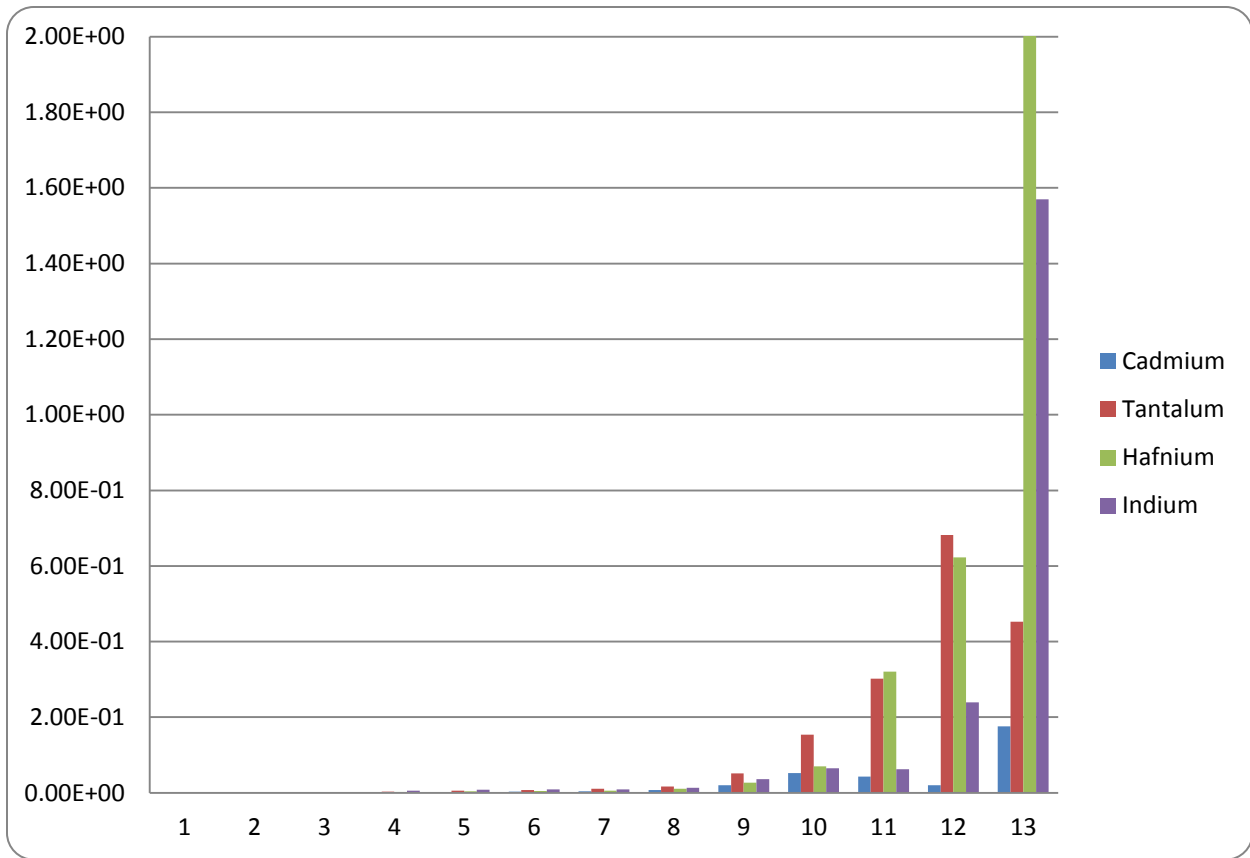


Figure 3.3b: Absorption cross section for groups 1 - 13 for: Cadmium, Tantalum, Hafnium, and Indium

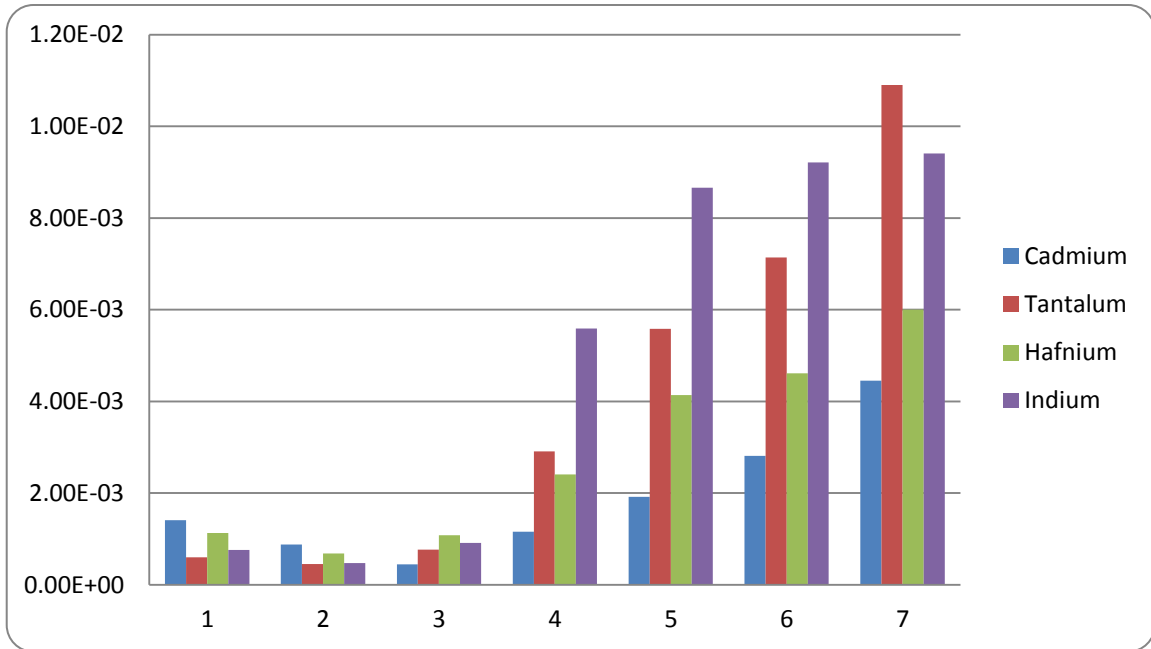


Figure 3.3c: Absorption cross section for groups 1 - 7 for: Cadmium, Tantalum, Hafnium, and Indium

Below are two plots taken from the metrics of completed Adjoint Run 3 with a level symmetric quadrature of S_{12} and P_2 . These plots examine the local convergence error versus the coarse mesh of the middle z-level of the model. This was done to determine if there was any highly localized error which could greatly increase run times, and could affect the convergence and iterative error of the surrounding zones via numerical diffusion. A graph of this in an Adjoint simulation for Adjoint energy group 1 – Forward group 30 – can be noted in Figure 3.4. The graph has four labeled points that have abnormally high error spikes – indicating presence of highly localized error. These four points correspond to the four labeled zones in Figure 3.5, where the zone labeled 1 corresponds to the Cadmium material zone.

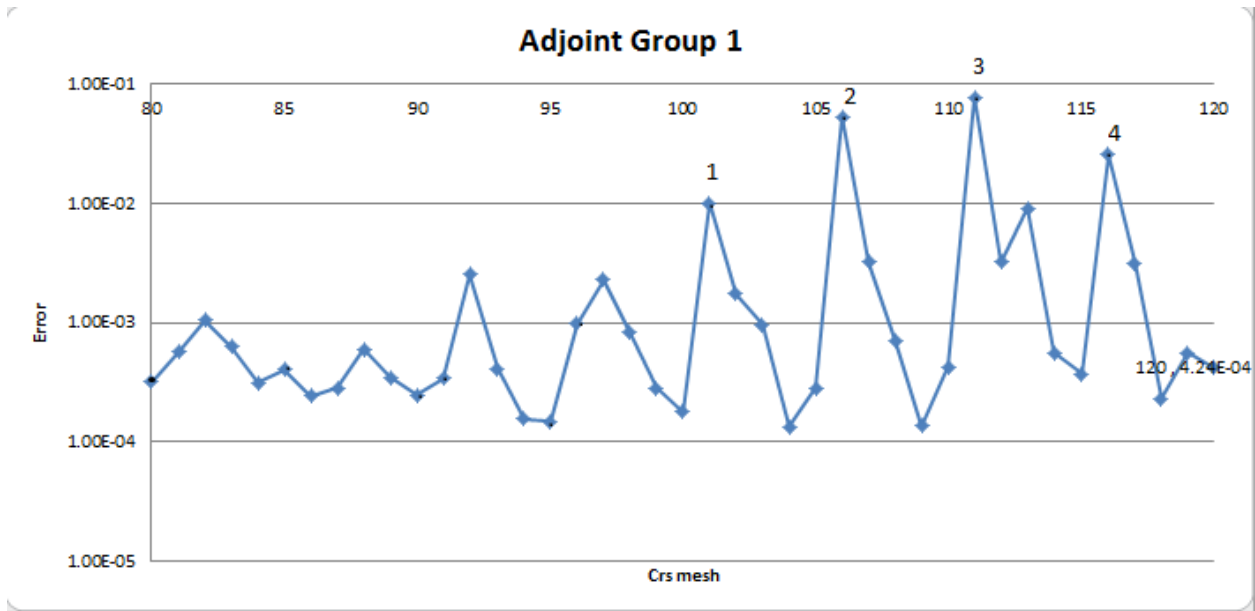


Figure 3.4: Adjoint group 1 error norm

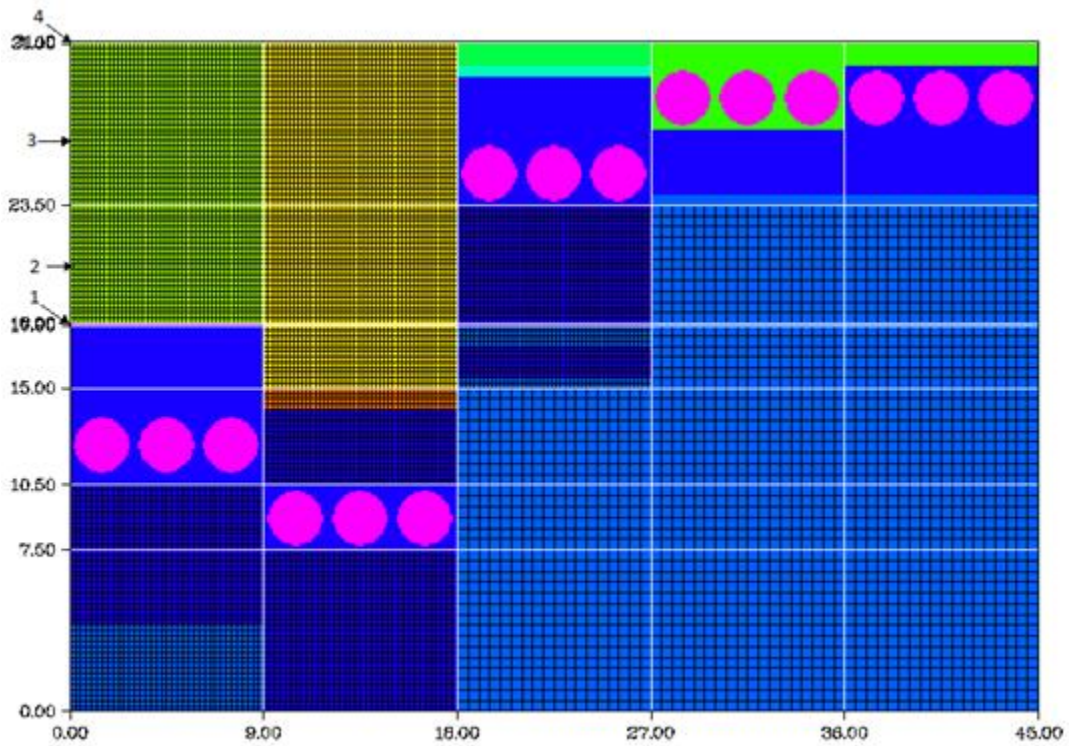


Figure 3.5: Detector model with 4 labeled zones, using the initial detector design

To understand how these errors are propagating, we need to evaluate the pathways related to neutron Adjoint importance. In Adjoint group 30, importance streams out of the detector located in Channel 1 and towards mesh 4. In the process, they will pass through the cadmium mesh – mesh 1. This introduces error into the problem that then propagates throughout the problem, and into adjacent meshes, as seen in Figure 3.4. Figure 3.6 shows the same error calculation, but for Adjoint group 30 – Forward group 1.

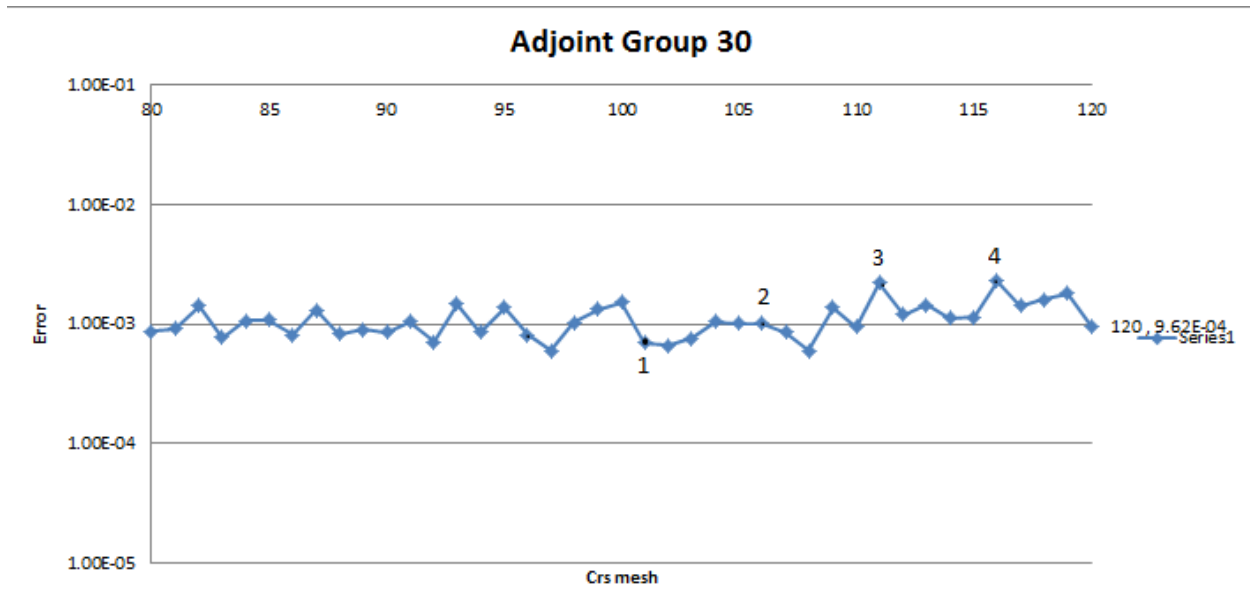


Figure 3.6: Adjoint group 30 error norm

Evaluating this graph shows that the cadmium does not add any additional convergence complications for neutrons on the high end of the energy spectrum since the absorption cross section for this energy group is significantly smaller. Similarly, but to a lesser degree, localized error propagation effects take place in detector blocks 2 and 3 due to the presence of tantalum, indium, and hafnium [8].

3.4. Cadmium Free Evaluation

To verify that the localized convergence error in the problem is caused by the presence of the cadmium strip, two additional simulations were performed. A new Forward and Adjoint

simulations were carried out using the initial test design; however, the cadmium strip was removed and replaced with an HDPE strip. The model was tested with S_{12} level symmetric quadrature, P_2 scatter cross sections, and an error tolerance of $< 1.0E-03$. The results for these simulations are shown in Table 3.5.

Table 3.4: Cadmium free Forward and Adjoint simulation

Run Type	Convergence Achieved
Forward	3.2 E-4
Adjoint	2.9 E-4

By removing the Cadmium strips, we note that both models converged completely, and were well within the error tolerance threshold. This result shows that the presence of the Cadmium strip indeed leads to convergence difficulty in the lowest energy neutron groups; however, this leaves the unresolved issue of how to proceed. The Cadmium could be removed from the model; however, the behavior of its absorption cross section is what introduces convergence difficulties, but it is also critical to detector functionality since the Cadmium provides essential scattering in high neutron energy regions [9]. Therefore the model will retain the Cadmium strip, but the zone that contains the Cadmium will require the number of fine meshes to be greatly increased – leading to the final detector design. This will help to reduce the error being propagated into the transport equation for both the Forward and Adjoint simulations. When the Cadmium bearing mesh cells refined significantly, convergence was satisfied.

3.5. Response Coupling Procedure

Now that the discrepancy in the convergence has been explained, the previous runs overall response counts will be evaluated [7]. However, before that can be done, a set of codes must be introduced that was created for this work. The two codes calculate the Forward and Adjoint responses that were obtained from the simulations – the full ‘react’ and ‘areact’ codes are presented in Appendices A-1 and A-2 respectively.

The Forward response calculation code – ‘react’ – does this calculation by multiplying the group flux in the detector (Φ) by the cross section for that energy group (σ) with the cell volume (V), and summing this over i cells in the detector, over all energy groups – Equation 3.1 [7].

$$R = \sum_{g=1}^G \sum_{i=1}^I \Phi_{i,g} \sigma_{i,g} V_i \quad [Equation 3.1]$$

The Adjoint response calculation is done using the code ‘areact’. The code performs this calculation by multiplying the Adjoint in the source region (Φ^*_d) with the source density (q), and the source volume (V), and summing this over i cells containing the source region, over all energy groups – Equation 3.2 [7].

$$R_a = \sum_{g=1}^G \sum_{i=1}^I \Phi^*_{a,g} q_g V_i \quad [Equation 3.2]$$

The accuracy of these two codes was verified by running a simplified detector model – Figure 3.6. This model was representative of a source detector response model; in this model the source is Dow-foam (green), the detector is 4 atm He-3 (pink), and the detector moderator assembly is polyethylene (blue). Two sets of Forward and Adjoint simulations were completed to verify the coupling of the detector response. The results of these simulations are presented in Table 3.7.

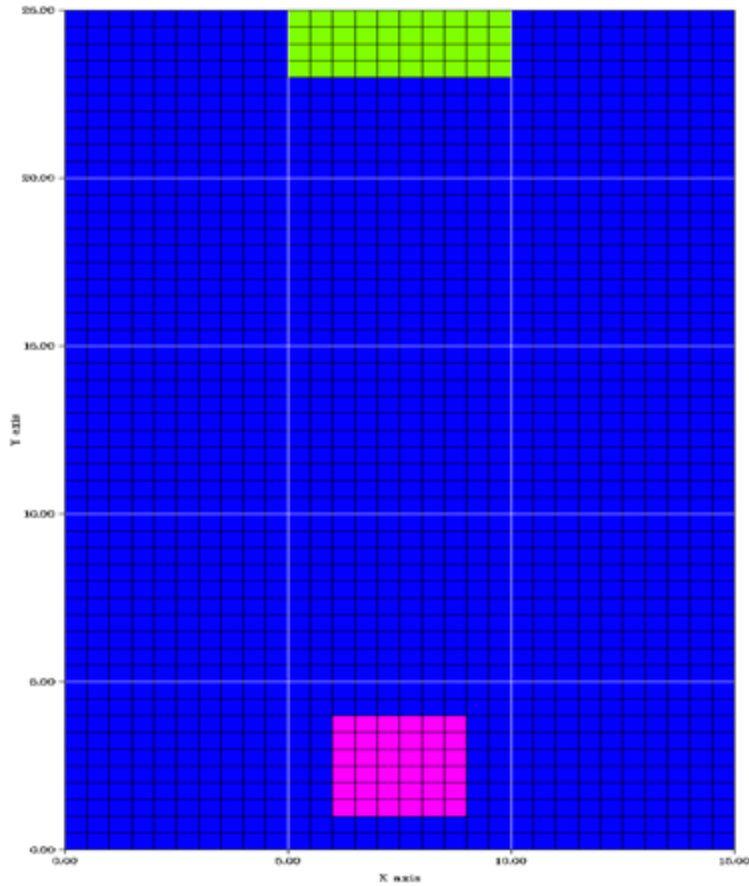


Figure 3.7: Simplified test model

Table 3.5: Test model results

Run Set	Run Type	Sn Order	Pn Order	Response (#/s)	Relative Difference
1	Forward	8	2	3.92E-03	.897
1	Adjoint	8	2	4.37E-03	
2	Forward	12	2	1.70E-02	1.01
2	Adjoint	12	2	1.69E-02	

The relative difference for this set of simulations was well within acceptable bounds, and as a result, it can be said that the Forward and Adjoint response are well converged for S_{12} level symmetric quadrature, validating the codes used to process the responses. This successful test

shows that the response count code is correct, and that direct coupling can be obtained with adequate phase space discretization, and proper meshing.

3.6. Separate Source Simulations

To couple the Adjoint response with a Forward source, several additional simulations are required. In this set of simulations, the detector was modeled five times in Adjoint mode, with each run only emitting particles from one of the five detector arrays, as seen in Figure 3.8.

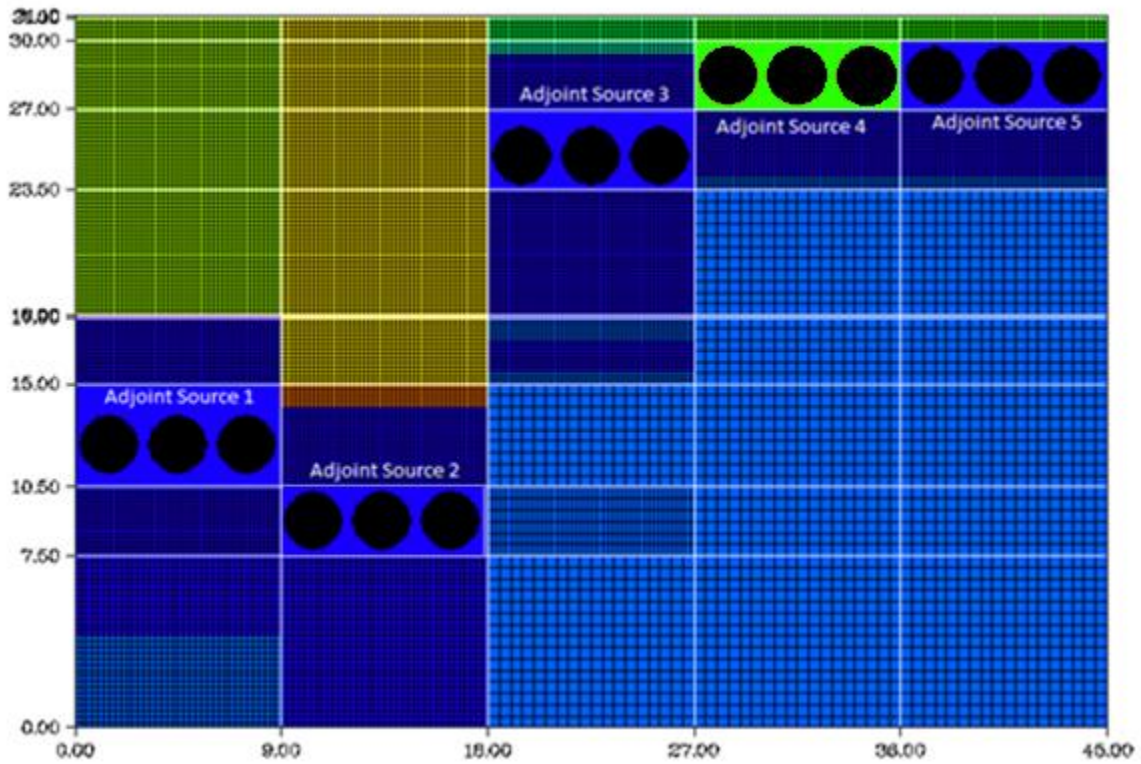


Figure 3.8: Separate Adjoint source simulations, each Adjoint source is labeled

The results obtained in these five simulations were used to generate the Adjoint leakage term required to find the average Adjoint response per detector array, as shown in Equation 3.3 [7].

$$R_a = \sum_{g=1}^G \sum_{i=1}^I J_{i,g}^\dagger q_{i,g} A_i \quad [\text{Equation 3.3}]$$

Where R_a is the Adjoint response [#s], $J_{i,g}^+$ is the Adjoint leakage per group, per mesh [unitless], and $q_{i,g}$ is the incident Forward source per group, per mesh [#cm²/s], and A_i is the surface area of the cell [cm²] [7]. The response that was generated for each of the five individual Adjoint simulations was collected across the entire top volumetric source of the detector array. The results for these simulations are presented in Table 3.7.

Table 3.6. Adjoint response, per source location, epithermal fission test source

Adjoint Source Location	Response (#/s)	Relative Response
Channel 1	4.61E-03 *	0.014%
Channel 2	.02151 *	0.065%
Channel 3	1.240	3.74%
Channel 4	18.1	54.57%
Channel 5	13.8	41.61%
TOTAL	33.17	100.00%

*Based on these results, it is noted that more than one set of Channels 1 and 2 may be required for statistically significant detection of neutrons with this source.

The total response for the five Adjoint runs summed to 33.17 counts per second for a fission test source. This number was then compared to the total counts from the previously performed Adjoint simulation with all detectors simultaneously emitting particles, and the results are presented in Table 3.8.

Table 3.7: Separate Adjoint model and full Adjoint model count comparison

Source/Run Type	Total Counts per sec	Ratio
Five Separate/Adjoint	33.17	.9978
One/ Adjoint	33.10	

The two Adjoint run sets both summed to approximately the same response value, showing that the individual runs performed using Adjoint transport were consistent with the previously performed full model simulation. This separate evaluation of the Adjoint simulation shows that both models converged to within targeted convergence limits [10].

3.7. Forward Surface Source Simulation and Adjoint Coupling

A final Forward simulation was performed where the source being used was a surface source. The 30 group source spectrum for a fission test source “painted” across the front surface of the detector as the surface source – this was performed to simulate a test incident source with a plutonium spectrum. The Forward simulation was carried out using an S_{10} level symmetric quadrature with P_2 scattering computation and a flux convergence tolerance of $1.0E-3$. The simulation was executed using PENTRAN, and the fluxes achieved convergence to $<1.0E-03$. The scalar fluxes in the detector tubes were then extracted and used in Equation 3.1 to generate a detector response.

The response generated was the total response in all fifteen detector tubes among the five channels spanning the model, and these results are presented in the first entry (run set 1a) of Table 3.9 (Adjoint results are discussed below).

Table 3.8: Surface source and Adjoint current test source comparison

Run Set	Run Type	Sn Order	Pn Order	Current Response (#/s)	Relative Ratio
1a	Forward Surface	10	2	33.14	.9999
1b	Adjoint Current	10	2	33.17	

To couple the detector system between the Forward and Adjoint simulations, the Adjoint response was tallied across all five detector channel blocks, and the total response is listed in Table 3.9 (run set 1b). We note that the total Adjoint response summed from relative contributions from each channel were almost identical to the Forward model response, revealing that the detector response in Forward mode is equal to the Adjoint response, as expected for fully

converged results. This confirms the complete consistency of the Forward and Adjoint simulations using the PENTRAN code system for this problem.

4. Validation Using Adjoint Current

Simulating the Adjoint response for each of the five individual detector blocks enabled us to individually attribute the relative response in each channel block. In addition, it also allowed us to obtain the neutron importance profile for each channel in order to accomplish a gross neutron spectroscopy for an arbitrary source term. This data was used to determine five mean energies (\bar{E}) for each separate Adjoint run corresponding to one of the five detector channels. The \bar{E} corresponds to the average energy of neutrons detected in that channel. These mean energies (\bar{E}) were calculated using Equation 4.1 [10]:

$$\bar{E} = \frac{\sum_{g=1}^{30} \sum_{i=1}^5 \Phi_{i,g}^{\dagger} E_g}{\sum_{g=1}^{30} \sum_{i=1}^5 \Phi_{i,g}^{\dagger}} \quad [\text{Equation 4.1}]$$

Where, $\Phi_{i,g}^{\dagger}$ is the scalar Adjoint function per front surface face [importance], per group, and E_g is the maximum or average energy for that bin [MeV]. For each \bar{E} calculation the flux for that the i-th coarse mesh and group g was multiplied by the respective group energy, the summation results were then normalized against the total flux for all 30 energy groups [10]. This created an energy range for incoming neutrons to cause a detection event in the He-3 detectors. Creating the range of \bar{E} values (\bar{E}_{max} to $\bar{E}_{average}$) allowed for the models detector channels to be individually tested with respect to the individual design. An example of the sample ranges for detector 1 is shown in Figure 4.1.

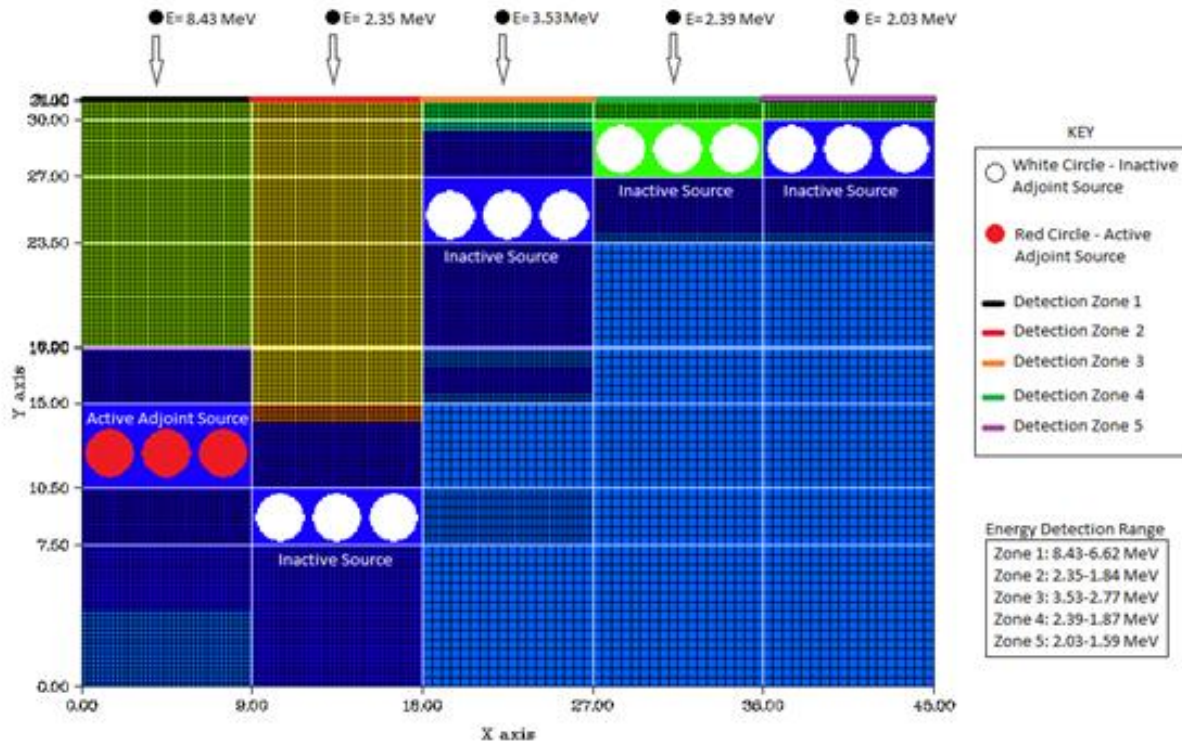


Figure 4.1: Maximum energy detection evaluation for Channels with an active Adjoint source placed on channel 1 (left-most block)

Note that Figure 4.1 depicts particles incident on each of the five separate detection channels due to the Adjoint source placed in Channel 1. We further point out that neutrons entering the front surface of other channels can ultimately cause an event in Channel 1, and the peak energies of the neutrons entering attributed to an event in Channel 1 are indicated in Figure 4.1. These particles will each cause a detection event in detector Channel 1, because they are within the detection range that was generated. A full set of detection energy ranges, relative to each of the five detectors was calculated, and is presented in Table 4.1.

Table 4.1: Energy detection ranges (MeV) for individual detector Channel blocks with corresponding Adjoint importance at that energy*

Source on Ch #	\bar{E} max/ \bar{E} avg, Adjoint	Detector Channel 1	Detector Channel 2	Detector Channel 3	Detector Channel 4	Detector Channel 5
1	\bar{E} max/ \bar{E} avg	8.43/6.62	2.35/1.84	3.53/2.77	2.39/1.87	2.03/1.59
1	Adjoint	7.97E-4	1.77E-3	1.01E-3	6.12E-4	3.64E-4
2	\bar{E} max/ \bar{E} avg	7.53/5.92	1.75/1.37	2.32/1.82	.451/.351	.247/.191
2	Adjoint	4.48E-4	1.43E-3	1.04E-3	1.14E-3	8.52E-4
3	\bar{E} max/ \bar{E} avg	2.11/1.64	.13/.101	.71/.554	.059/.046	.118/.091
3	Adjoint	3.02E-3	2.79E-2	1.13E-2	1.81E-2	6.12E-3
4	\bar{E} max/ \bar{E} avg	3.72/2.9	.432/.336	.151/.117	1.36E-3/ 1.03E-3	2.93E-3/ 2.21E-3
4	Adjoint	1.86E-4	1.65E-3	3.98E-03	6.42E-2	2.54E-2
5	\bar{E} max/ \bar{E} avg	4.7/3.7	.811/.631	.197/.154	2.99E-3/ 2.25E-3	8.75E-4/ 6.54E-4
5	Adjoint	3.37E-5	2.69E-4	1.19E-3	2.6E-2	6.58E-2

*All energies are in MeV

Table 4.1 enables us to see the detection capabilities of the model, and it also makes it apparent that the channel blocks are functioning as they were designed to with regard to neutron energy sensitivity. Each of the Channels targeted responses can also be seen – highlighted in yellow in Table 4.1. The Maximum and Average incident neutron energy to cause a response for each of the Detectors when the source is located above the target channel can be seen in Figures 4.2 and 4.3 respectively.

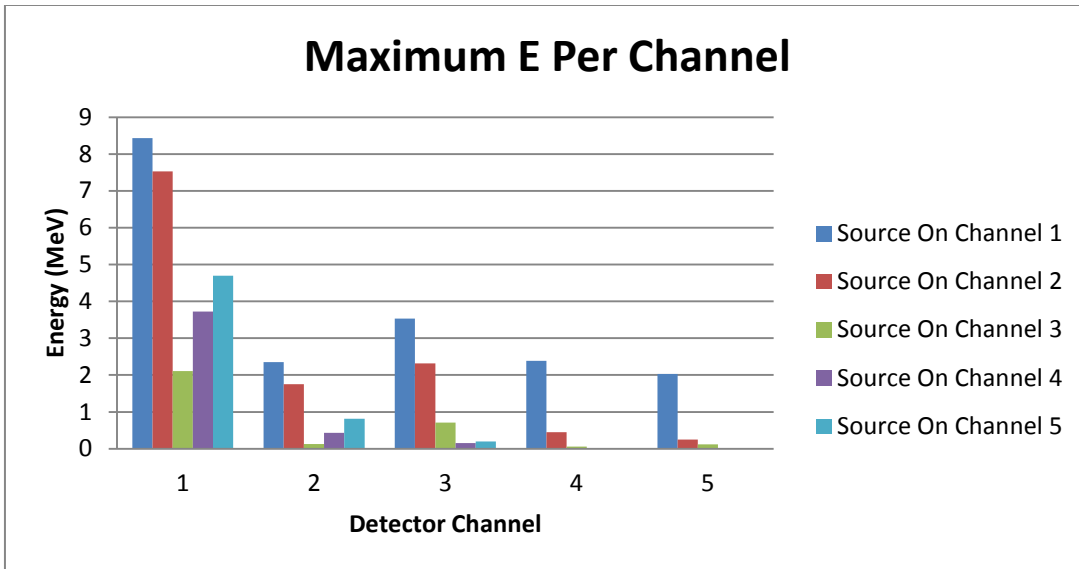


Figure 4.2: Maximum neutron energy to cause a detection event within a Channel for a source placed at each Channel location

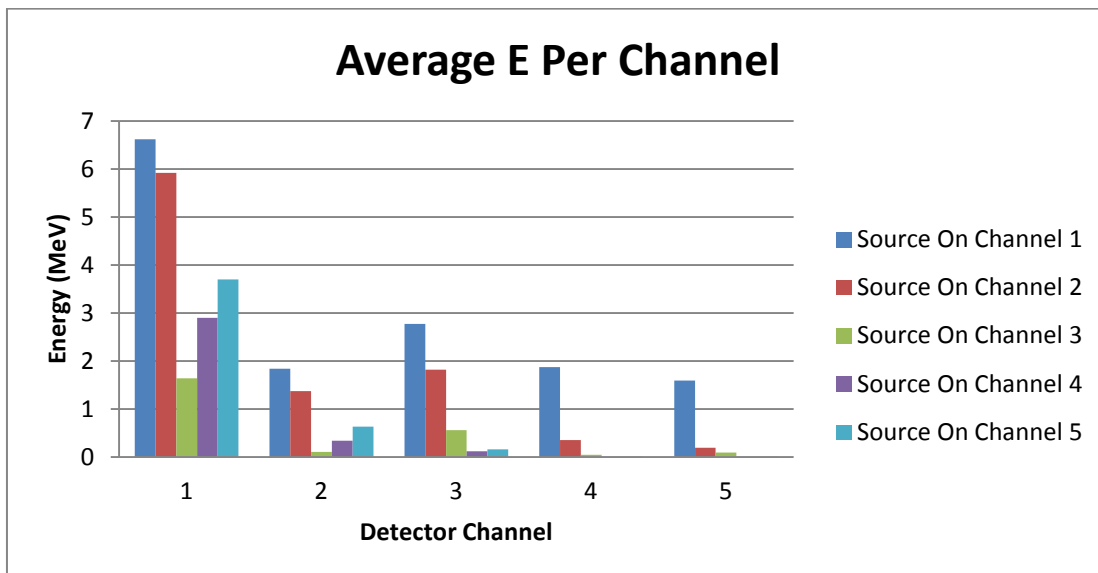


Figure 4.3: Average neutron energy to cause a detection event within a Channel for a source placed at each Channel location

In addition, Table 4.1 also gives a tabulated breakdown of the full detection capabilities of each of the individual detector blocks.

- Detector Channel 1 will be able to register incident neutrons in the high MeV range (1.59 MeV to 8.43 MeV).
- Detector Channel 2 will register neutrons in the mid to high MeV range (7.53 MeV to 0.191 MeV).
- Detector Channel 3 will register neutrons in the low MeV range (2.11 MeV to .091 MeV).
- Detector Channel 4 can register neutrons in the epithermal range (3.72 MeV to 1.03E-3 MeV)*.
- Detector Channel 5 can register neutrons incident on the detector surface within the epithermal - to thermal range (4.7 MeV to 6.54E-4 MeV)*.

*Detector Channel's 4 & 5 are able to register neutrons outside of their designed energy range; however, taking the adjoint importance into account when reviewing Table 4.1 shows that events in these Channels are highly unlikely for fast neutrons. (A more complete discussion of adjoint importance is given below). For the detector in Channel 4, the adjoint importance for incident high-energy neutrons on Channel 1's face is several orders of magnitude lower than the adjoint importance for epithermal neutrons that are incident on the detector face. A similar relationship exists for high energy neutrons arriving on the detector face, and causing an event in Channel 5. Utilizing this information Channel's 4 & 5 detection ranges can be revised to:

- Detector Channel 4's detection events are likely from neutrons in the epithermal range (2.93E-3 MeV to 1.03E-3 MeV).
- Detector Channel 5's detection events are likely from neutrons incident on the detector surface within the epithermal - to thermal range (2.99E-3 MeV to 6.54E-4 MeV).

All of this information shows that the individual blocks are also functioning as they were initially designed. In addition to verifying the functionality of the detector system, the Adjoint for each of the source/channel combinations reveals the relative likelihood of a source at each location to cause an event in that detector. Graphs of the Adjoint Importance in each Channel when the source is located over Channels 1 or 2 is shown below in Figure 4.4, and for when the source is located over Channels 3,4, or 5 is shown in Figure 4.5 respectively.

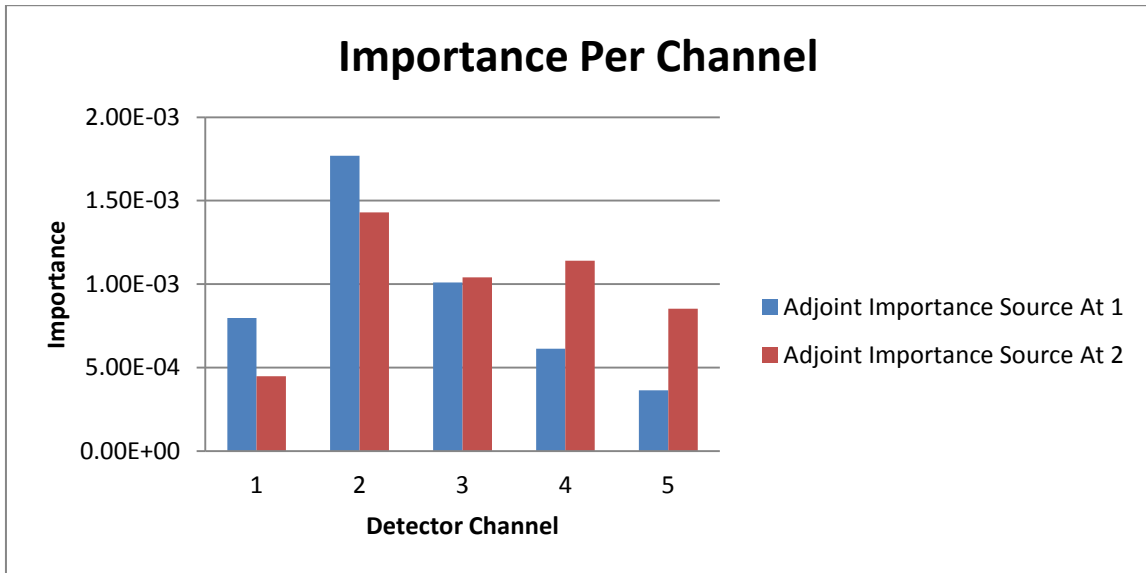


Figure 4.4: Adjoint importance for Channels 1-5 when the source is located at Channel 1 or

2

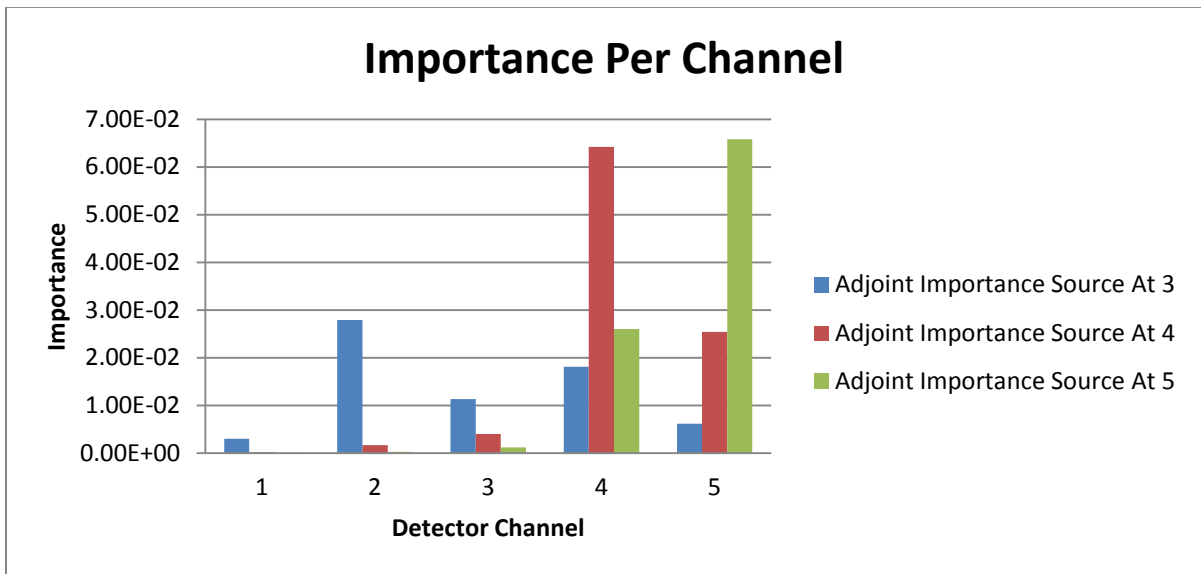


Figure 4.5: Adjoint importance for Channels 1-5 when the source is located at Channel 3, 4,

or 5

For example, as shown in Figure 4.4, the case of the source being located at Channel 1's detector, it can be seen from the table that the Adjoint importance for Detector Channel 1 is:

7.97E-4, and for the source located at Detector Channel 2 it is: 1.77E-3. Detector Channel 2 has an Adjoint importance two times greater than Detector Channel 1 for causing an event in Detector 1. This indicates that neutrons incident on Channel 2 with energy between 2.53 MeV and 1.84 MeV are twice as likely to cause a detection event in Channel 1's detector, than a neutron incident on Channel 1 with energy between 8.43 MeV and 6.62 MeV. However, for unique high energy sources this same relationship would not hold true. A source of 14.1 MeV neutrons will cause more events in Detector Channel 1 than Detector Channel 2. This information is critical to how the spectroscopy of the assembly will be evaluated; because of this the counts registered in Channel 1's detector could be from incident neutrons from either Channel 1, 2, or 3. However, the information provided by this Channel's detector will still be relevant, because the detector in Channel 1 will only register particles with energy greater than 1.8 MeV. This information will also be useful in the next phase of research, spectroscopy of individual neutron sources in a realistic road side scenario.

5. SOURCE DETERMINATION

5.1. MCNP5 Simulation

Using the individual block Adjoint currents obtained in the previous Chapter, the response from each channel for any arbitrary new sources can be determined so long as the initial source strength or incident current is known. Using a “hybrid” Monte Carlo-Sn Adjoint approach, we can first determine the current of particles crossing each detector module plane (such as using Monte Carlo based on the model presented in Figure 2.7 using MCNP5). The detector response rate can then be calculated for this scenario by coupling the Monte Carlo results with the Sn Adjoint leakage on the front detector surface. To proceed further and distinguish between the types of neutron sources that one may encounter, we have evaluated several sources using this hybrid approach:

- 83.5g Am-Be spherical neutron source – initial isotropic strength: $1.26\text{E}+08$ [#s], modeled as a small spherical source using Monte Carlo; a total of $9.35\text{E}+04$ n/s strike each channel at centerline
- 5 μg Cf-252 neutron source – initial isotropic strength: $6.38\text{E}+09$ [#s], modeled as a small point source using Monte Carlo; a total of $4.50\text{E}+06$ n/s strike each channel at centerline
- 21g Pu-Be solid sphere – initial isotropic strength: $1.09\text{E}+06$ [#s]; a total of $7.90\text{E}+02$ n/s strike each channel at centerline
- 14.1 MeV point source – initial isotropic strength: $1.0\text{E}+11$ [#s]; a total of $6.43\text{E}+07$ n/s strike each channel at centerline
- 8kg WGPu Sphere – initial isotropic strength: spontaneous source $5.06\text{E}+05$ [#s]. with a $k_{\text{eff}} = .948$, for a full source leakage strength of: $6.05\text{E}+06$ [#s]; a total of $4.30\text{E}+03$ n/s strike each channel at centerline

The objective in using these different sources in the realistic MCNP5 model is to determine if the source can be discriminated using the relative counts registered in each detector for gross detector spectroscopy to ascertain the original source spectrum. To accomplish this, the

neutron emission spectra for our 30 group structure for each source was determined using the ORIGEN code [11]. The spectrum was obtained as binned energy groups, and is graphed against each group respective flux in Figures 5.1, 5.2, and 5.3, respectively – no emission spectra is displayed for the 14.1 MeV source, because it is a mono-energetic emission at 14.1 MeV.

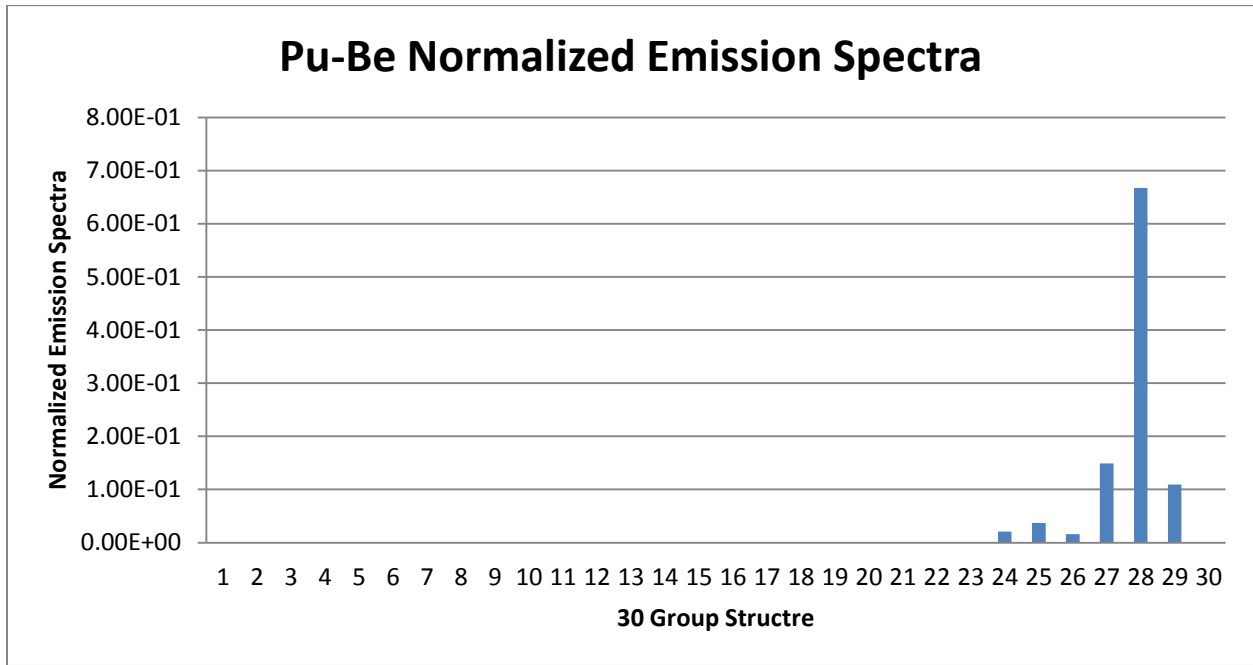


Figure 5.1: 1 Ci Pu(WGPu) -Be Normalized source emission spectrum in the 30 group structure

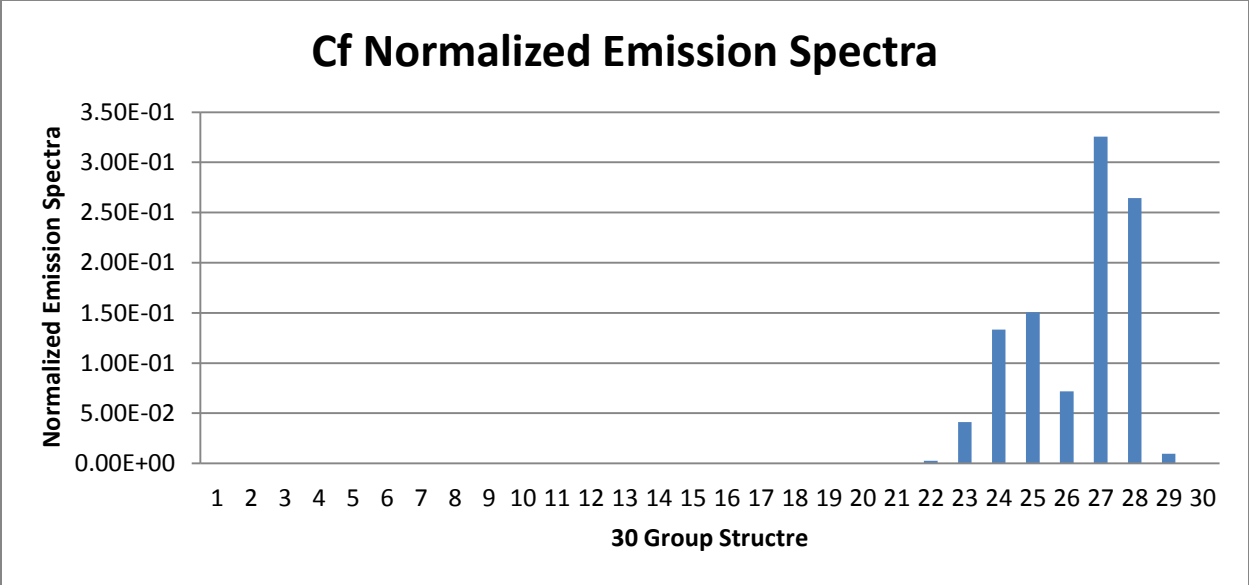


Figure 5.2: 2.7E-03 Ci Cf Normalized source emission spectrum in the 30 group structure

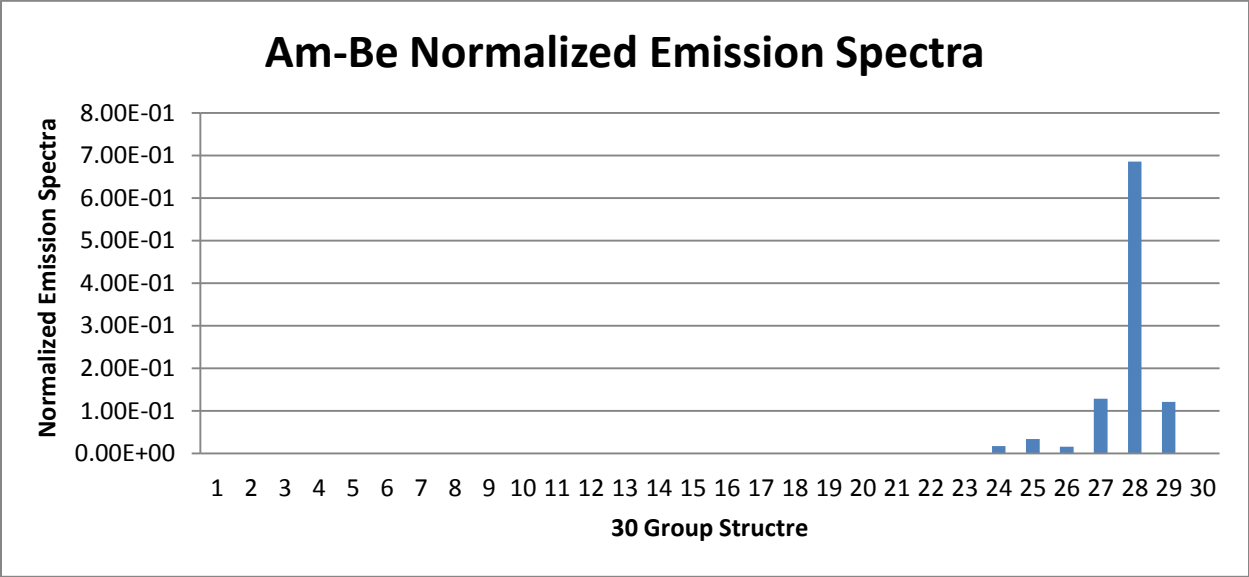


Figure 5.3: 50 Ci Am-Be Normalized source emission spectrum in the 30 group structure

These source spectra were defined into a continuous energy MCNP5 model similar to that depicted in Figure 2.7, and the two neutron tallies were collected for each of the source simulations. A surface tally was used across the detector face to register the particles crossing into the detector. An example of what this surface tally looked like in MCNP5 can be seen in Figure 5.4. The surface tally was used to determine the particle fluence reaching the detector face

from the vehicle and gather the needed $q_{i,g}$ term for use in Equation 3.2 [12]. Coupling the MCNP5 surface tally and the Adjoint current obtained in the PENTRAN simulations gave a hybrid Adjoint response for the detector system, on a “per source particle” basis. Multiplying this final channel-based response by each of the respective source strength in a channel projected onto each individual Channel surface area (54 cm^2) gave a final Adjoint response for each of the simulations, shown below in Table 5.1. To generate the Forward response, a tally was used to determine the reaction rate across the five detector channels [12]. The volumetric tallies were placed as shown in Figure 5.4. The results from the Monte Carlo calculation are given in Table 5.1.

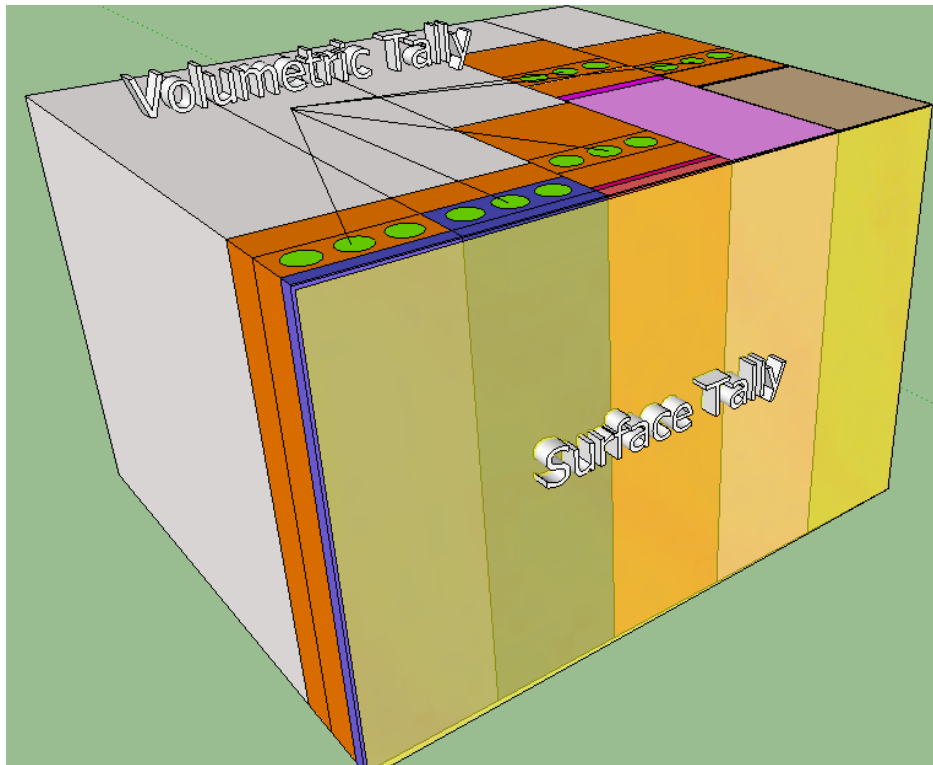


Figure 5.4: Surface and Volumetric Tally for the Detector Model

Table 5.1: MCNP5 tally responses, for various sources, and relative errors

Source	Response Type	Response Location	Response (#/s)	Rel Error
Am-Be	Adjoint Response:	Channel 1 Adjoint	1.69	0.0004
		Channel 2 Adjoint	1.62	0.0004
		Channel 3 Adjoint	13.06	0.0004
		Channel 4 Adjoint	17.51	0.0004
		Channel 5 Adjoint	14.36	0.0004
		Total Adjoint Response	48.24	0.0004
	Forward Response	Channel 1 He-3 Tubes	3.82	0.0028
		Channel 2 He-3 Tubes	4.64	0.0025
		Channel 3 He-3 Tubes	22.58	0.0012
		Channel 4 He-3 Tubes	10.77	0.0014
		Channel 5 He-3 Tubes	9.59	0.0017
		Total Forward Response	51.4	0.0028
Pu-Be	Adjoint Response:	Channel 1 Adjoint	1.41E-02	0.0004
		Channel 2 Adjoint	1.33E-02	0.0004
		Channel 3 Adjoint	1.03E-01	0.0004
		Channel 4 Adjoint	1.43E-01	0.0004
		Channel 5 Adjoint	1.17E-01	0.0004
		Total Adjoint Response	3.9E-01	0.0004
	Forward Response	Channel 1 He-3 Tubes	3.26E-02	0.0028
		Channel 2 He-3 Tubes	4.02E-02	0.0026
		Channel 3 He-3 Tubes	1.86E-01	0.0012
		Channel 4 He-3 Tubes	8.73E-02	0.0015
		Channel 5 He-3 Tubes	7.68E-02	0.0017
		Total Forward Response	4.2E-01	0.0028
Cf	Adjoint Response:	Channel 1 Adjoint	8.02E+01	0.0004
		Channel 2 Adjoint	8.57E+01	0.0004
		Channel 3 Adjoint	7.57E+02	0.0004
		Channel 4 Adjoint	9.40E+02	0.0004
		Channel 5 Adjoint	7.69E+02	0.0004
		Total Adjoint Response	2632	0.0004

Table 5.1 Continued

	Forward Response	Channel 1 He-3 Tubes	1.69E+02	0.003
		Channel 2 He-3 Tubes	1.99E+02	0.0028
		Channel 3 He-3 Tubes	1.31E+03	0.0011
		Channel 4 He-3 Tubes	6.38E+02	0.0013
		Channel 5 He-3 Tubes	5.88E+02	0.0015
		Total Forward Response	2906	0.0028
14.1 MeV	Adjoint Response:	Channel 1 Adjoint	6.96E+00	0.0012
		Channel 2 Adjoint	6.57E+00	0.0012
		Channel 3 Adjoint	3.87E+00	0.0012
		Channel 4 Adjoint	3.31E+00	0.0012
		Channel 5 Adjoint	3.09E-01	0.0042
		Total Adjoint Response	21.0	0.0042
	Forward Response	Channel 1 He-3 Tubes	8.71E+00	0.009
		Channel 2 He-3 Tubes	4.01E+00	0.0084
		Channel 3 He-3 Tubes	3.23E+00	0.0051
		Channel 4 He-3 Tubes	3.07E+00	0.006
		Channel 5 He-3 Tubes	2.66E+00	0.0074
		Total Forward Response	21.7	0.009
8kg WGPu	Adjoint Response:	Channel 1 Adjoint	1.27E+02	0.0008
		Channel 2 Adjoint	1.43E+02	0.0008
		Channel 3 Adjoint	1.33E+03	0.0008
		Channel 4 Adjoint	1.57E+03	0.0008
		Channel 5 Adjoint	1.28E+03	0.0008
		Total Adjoint Response	4447	0.0008
	Forward Response	Channel 1 He-3 Tubes	2.16E+02	0.0063
		Channel 2 He-3 Tubes	2.53E+02	0.0058
		Channel 3 He-3 Tubes	1.94E+03	0.0022
		Channel 4 He-3 Tubes	9.57E+02	0.0025
		Channel 5 He-3 Tubes	8.98E+02	0.0029
		Total Forward Response	4263	0.0063

As seen in Table 5.1, all tally errors were within the acceptable limits. Table 5.1 also shows the individual responses – $R_{a,Channel\ 1} \neq R_{f,Channel\ 1}$ – for each of the five tested sources, do not match up on channel by channel case; however, the total Adjoint and Forward responses – $R_{a,Net} = R_{f,Net}$ – do couple within acceptable limits. The total response coupling for each of the five sources is shown below in Table 5.2

Table 5.2: MCNP5 Forward response and PENTRAN model Adjoint response

Source	Response type	Total Response (#/s)	Coupling Ratio (Ra/Rf)
Am-Be	Ra -Adjoint	48.24	.9385
	Rf- Forward	51.40	
Pu-Be	Ra - Adjoint	0.39	.9222
	Rf - Forward	0.42	
Cf	Ra - Adjoint	2632	.9056
	Rf - Forward	2906	
14.1 MeV	Ra - Adjoint	21.0	.9700
	Rf - Forward	21.7	
8kg WGPu	Ra - Adjoint	4447	.9585
	Rf - Forward	4263	

Comparing the Forward and Adjoint responses for each of the runs as a ratio of Adjoint response to Forward response, gives at least a 90% response ratio. This is reasonable, and demonstrates that the Adjoint current can be used to accurately determine the detector response when only the source distribution incident on the detector assembly or “incident source strength”, is known. In addition, the difference between the Channel responses shows the amount of ‘intra-Channel’ leakage that occurs during detection. The Adjoint response gives the ideal neutron detection for each of the individual detectors, where the source is projected directly onto the respective detector channels face. In the case of the Adjoint the internal neutron physics of the detectors has already been determined by way of the Adjoint current. While the Forward response shows the ideal detection, allowing neutrons to travel through the detector and in-between individual Channels. By knowing the amount of ‘intra-Channel’ leakage that occurs during detection, the model could be further refined – through the addition of new barrier

materials – to optimize the detector until the relationship of $R_{a,Channel 1} = R_{f,Channel 1}$ can be achieved.

5.2. Initial Spectrum Determination Using Ratio Method

With the three sources coupled with consistent results, the next phase of this effort is to determine if the responses from the different channels can be used to differentiate between the various neutron sources. First the three sources must be compared to determine the relative difference in their emission spectra. This is done by normalizing the sources and plotting them together using the same energy bin structure as before. The results of this comparison are presented below in Figure 5.5.

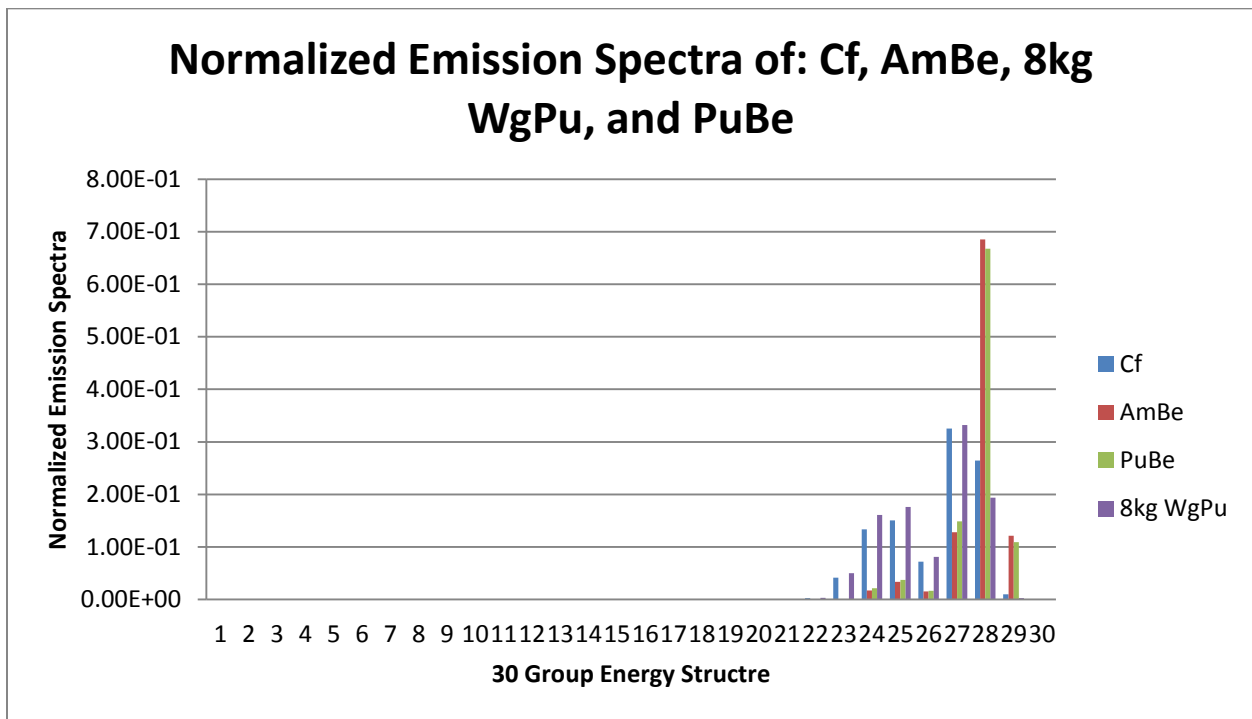


Figure 5.5: Cf-252, 14.1 MeV, Pu-Be & Am-Be Normalized source emission spectra comparison

It is readily apparent from Figure 5.5 that the AmBe and PuBe sources are close in spectral behavior, and emit more overall particles in the 10-20 MeV energy range than the Cf. Therefore, we should see an increased detector response for the AmBe and PuBe sources, and a

decreased response for the Cf source in Channel 1 detectors. However, Cf emits more particles in the 0.1-3 MeV range; therefore, we should see a slight difference between the Cf and AmBe/PuBe responses in the detectors located in Channels 4 & 5. The 14.1 MeV source should see the largest response of the other three sources in Channel 1 & Channel 2. The normalized flux responses for each of the sources are shown in Table 5.3.

Table 5.3: Normalized channel counts

Source	Channel 1 Response (#/s)	Channel 2 Response (#/s)	Channel 3 Response (#/s)	Channel 4 Response (#/s)	Channel 5 Response (#/s)
Am-Be	.074	.090	.439	.210	.187
Cf-252	.058	.069	.451	.22	.202
Pu-Be	.080	.100	.440	.210	.180
14.1 MeV	.331	.312	.184	.157	.0147
8kg WGPu	.051	.059	.454	.225	.211

The response difference is not as pronounced as was expected, and this could be make identifying sources more difficult. To alleviate some of these initial difficulties, a ratio technique is proposed using different channel responses to enhance the difference between the channels more pronounced. Creating a ratio for the number of neutrons that were detected (Channel 1) within the energy range of : 1.59 MeV to 8.43 MeV, to the number of neutrons detected (Channel 3) within the energy range of: 2.11 MeV to .091 MeV, we can generate a ratio to look at the different relative energy detections, as presented in Table 5.4.

Table 5.4: Channel 1 count ratios relative to Channel 3

Source	Channel 1 / Channel 3
Am-Be	.169
Cf-252	.129
Pu-Be	.182
14.1 MeV	1.80
8kg WGPu	.111

From Table 5.4 it can be seen that there is a significant difference in the ratio of neutrons detected by Channel 1 versus the number of neutrons detected by Channel 3. This ratio shows the general difference in detection magnitudes for the various Channels for each of the sources. For example: for every 1 neutron detected in Channel 3, 0.169 neutrons will be detected in Channel 1 for the Am-Be source; however, because neutron counts must be integers, for every 6 neutrons detected in Channel 3, 1 neutron will be detected in Channel 1 for the Am-Be source. Using this method shows that the Am-Be & Pu-Be sources will register approximately 6 neutrons in the 2.11 MeV to 0.091 MeV range for every 1 neutron detected in the 1.59 MeV to 8.43 MeV range. While the Cf source will register 8 neutrons in the 2.11 MeV to .091 MeV range for every 1 neutron detected in the 1.59 MeV to 8.43 MeV range. This indicates that the Cf source is emitting more neutrons in the 2.11 MeV to .091 MeV range relative to the Am-Be or Pu-Be sources. The 14.1 MeV source has a ratio of 1.8, indicating that for every 9 particles detected in Channel 1, 5 particles will be detected in Channel 3. This shows that for even a purely fast neutron source, some particles will be detected in other channels. This is attributed to neutrons being moderated by scattering through the car body, components, and road surface. As expected, this does indicate that the 14.1 MeV source is emitting more neutrons in the extreme fast spectrum, $E > 8.43$ MeV, than in the 2.11 MeV to .091 MeV range. Expanding this ratio method for all four detector Channels gives us Table 5.5.

Table 5.5: Channel count ratios relative to Channel 3

Source	Channel 1 / Channel 3	Channel 2 / Channel 3	Channel 4 / Channel 3	Channel 5 / Channel 3
Am-Be	.169	.205	.477	.425
Cf-252	.129	.152	.486	.448
Pu-Be	.182	.227	.477	.409
14.1 MeV	1.80	1.69	.854	.0796
8kg WGPu	.111	.131	.494	.463

Comparing the results of Table 5.5 with Figure 5.5, it can be seen that the relative counts are different for the sources individual spectrums. The Cf -252 has a decreased response from

Channels 1 and 2; however, it has a slightly increased response in Channels 4 and 5. This ratio method makes it easier to see the apparent difference between the WGPu / AmBe / PuBe emission spectra compared to that of the Cf-252, but it doesn't show any immediate difference between the similar emission spectra of the: WGPu, PuBe or AmBe sources. This can be achieved by setting up a different set of ratios.

A second set of ratios that was investigated used Channel 2 as a reference, neutrons within the energy range: 7.53 MeV to 0.191 MeV. The set of ratios was computed for all three sources, and the results are presented in Table 5.6.

Table 5.6: Channel count ratios relative to Channel 2

Source	Channel 1 / Channel 2	Channel 3 / Channel 2	Channel 4 / Channel 2	Channel 5 / Channel 2
Am-Be	0.82	4.87	2.32	2.07
Cf-252	0.85	6.58	3.20	2.95
Pu-Be	0.80	4.40	2.10	1.80
14.1 MeV	1.06	.590	.504	.047
8kg WGPu	.85	7.67	3.78	3.55

The difference between the WGPu, AmBe, and PuBe emission spectra can be seen here, but may be improved. A final ratio was established, using the high energy fast neutron detector counts as the reference (Channel 1). The results of this ratio exercise can be seen in Table 5.7.

Table 5.7: Channel count ratios relative to Channel 1

Source	Channel 2 / Channel 1	Channel 3 / Channel 1	Channel 4 / Channel 1	Channel 5 / Channel 1
Am-Be	1.21	5.91	2.82	2.51
Cf-252	1.18	7.77	3.78	3.48
Pu-Be	1.25	5.50	2.63	2.25
14.1 MeV	.943	.557	.475	.0443
8kg WGPu	1.17	8.97	4.43	4.16

This comparison highlights the differences in the various spectra. Referring back to Figure 5.5, it can be seen that the AmBe source emits slightly more fast neutrons than the PuBe source, which is highlighted in the ratio of Channel 5 to Channel 1. Table 5.7 highlights the fact that the 8kg WGPu source emits more low energy fast neutrons than either the PuBe or AmBe sources. Table 5.7 also makes it apparent that the 14.1 MeV source emits no thermal neutrons. The ratio method applied to the 14.1 MeV source shows that for every 22 neutrons detected in Channel 1, 1 neutron is detected in Channel 5. This indicates that the neutron detectors could be used in series to detect differences in source emission spectra. The AmBe and PuBe sources have very comparable emission spectra; however, the detector responses for the different channels identify those differences, and mirror the differences in their respective emission patterns. Overall, these studies indicate differences in relative detector response for different sources, and different emission spectra.

6. DRIVE BY DETECTION SIMULATION

6.1. Field of View

With a verification of the forward and adjoint responses, the system's ability to detect a mobile source will be investigated. As noted previously, a detector field of view must be investigated and established. The Field of View (FOV) is the range within the detector module that the SNM will generate a measurable response [13]. The maximum response that can be generated by the SNM will be when the SNM is located at the position $x = 0$ cm in the detector FOV – that is, when the source is directly in front of the detector [13]. A figure showing the detector FOV is shown in Figure 6.1 [13].

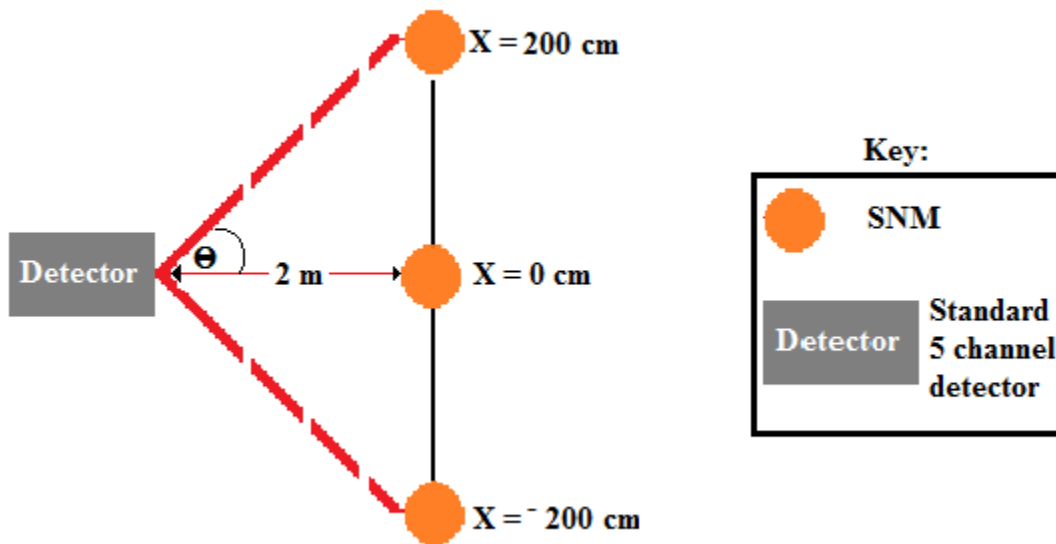


Figure 6.1: Detector FOV in a road side scenario

To maximize the signal to noise ratio for the detection system, the system requires that the detector aperture only be open while the SNM is within the FOV. For this application, the FOV is therefore determined to be 4m (200 cm before the detector center line, and minimum slant range distance to a single detector assembly, and 200 cm thereafter).

6.2. F-Factor

The scenarios that will be considered will use this prescriptive FOV were optimized earlier in the scenario investigation. The car, with the SNM in the trunk, will be observed by the detector only within the 4m window for each channel, and should be achievable with suitable timing or a RFID switch. Using this assumption, we can begin to solve for the “F-factor” (F_{factor}), a transport correction factor that can be used to estimate the number of particles that will travel uncollided to the detector face for a given source strength.

In a given instant, the number of uncollided neutrons can be estimated, on a per second basis, at a correlative location ‘x’ – as seen in Figure 6.1 – using Equation 6.1 [1].

$$R_g(x) = \frac{(S_g)}{4\pi(z_0^2 + x^2)} A_d \cos \theta = \frac{(S_g)}{4\pi(z_0^2 + x^2)} \frac{(A_d \cdot z_0)}{(z_0^2 + x^2)^{1/2}} \quad [\text{Equation 6.1}]$$

Where:

- $R_g(x)$ is the incident neutron rate for energy group g for an SNM source located at some position within the FOV: x (#/sec);
- S_g is the number of neutrons emitted from the SNM for group g (#/sec);
- A_d is the detector area on the front surface e.g. ($A_d = 9cm * 30cm = 270cm^2$);
- θ is the half of the detector-FOV angle
- z_0 is the half lane width ($z_0 = 200cm$).
- $x = v_0 t$, where the distance from SNM to the center of FOV is x , and where v_0 is the car speed;

Where we note that $\frac{(A_d \cdot z_0)}{(z_0^2 + x^2)^{1/2}}$ is the cosine-projected detector front surface area viewed relative to the detector-SNM direction [13]. With this in mind, Equation 6.1 will only represent the uncollided incident neutrons at the front surface for each position – if we assume the SNM is a point source [13]. This assumption will be valid for the current case, because an SNM that would fit inside a vehicle trunk would be small, and the distance from the vehicle to the detector will be relatively large. Equation 6.1 will be used in the calculation of the F-factor, which is defined in Equation 6.2 [13].

$$F_{factor} = \frac{R_{collided}}{R_{uncollided}} \quad [\text{Equation 6.2}]$$

The F_{factor} – defined as the ratio of collided to uncollided particles – can be used to determine the amount of collided particles in the system given only the initial source strength. To generate the R_{collided} term for use in Equation 6.2, several additional simulations were required. The series of eight simulations, in which the source is moving in 50 cm intervals with respect to the detector model, were created for this purpose. An example of this can be seen in Figure 6.2, where a vehicle with an SNM in its trunk, moves through the 8 intervals.

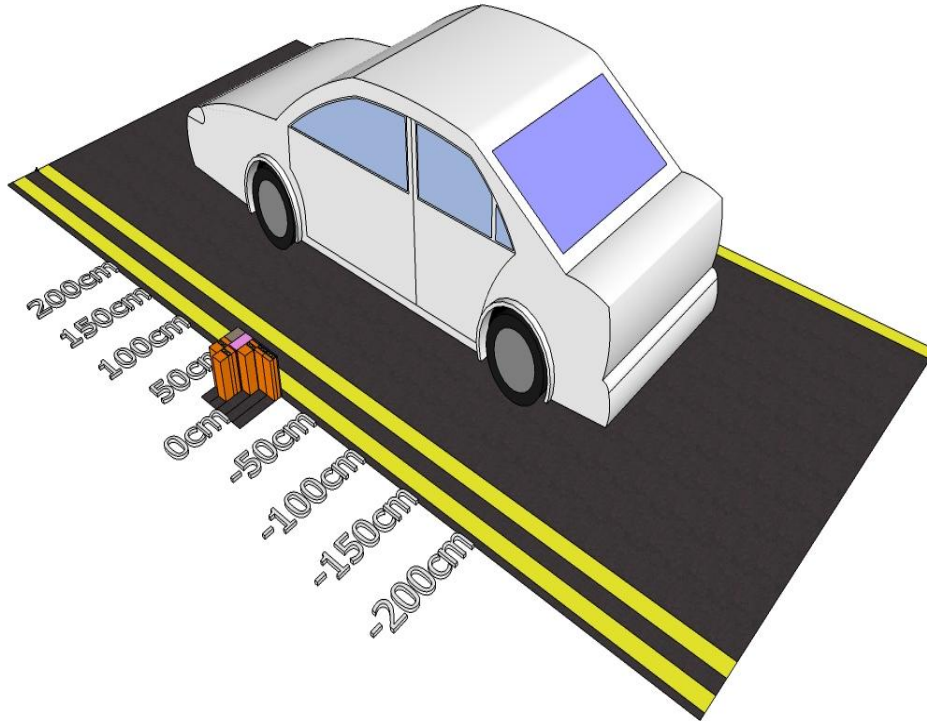


Figure 6.2: Mobile SNM Interval Breakdown at Eight Sampling Points along Vehicular Travel

The source chosen to be used in these simulations was the PuBe source. This source was selected because its overall response was the weakest of three tested sources, and evaluation of the system against the weakest source will help insure functionality and stability. The surface tallies for the eight detection evaluations/simulations were set up the same way as the previous MCNP5 simulation – with a surface and volumetric tally – the only change between the runs is the relative position of the center of the source with respect to the detector’s FOV. The eight simulations were completed, and the results of the runs are displayed below in Table 6.1.

Table 6.1: MCNP5 tally responses for a 1.09E6 n/s PuBe source, and relative errors for 8 road side positions in simulations surrounding the center line for the vehicle

Tally	Vehicle C/L Position, cm	Location	Response [#s]	Relative Error
Volumetric	-200	Channel 1 He-3 Tubes	4.45E-02	2.4 E-3
		Channel 2 He-3 Tubes	2.24E-02	3.4 E-3
		Channel 3 He-3 Tubes	5.83E-02	2.2 E-3
		Channel 4 He-3 Tubes	2.18E-02	2.9 E-3
		Channel 5 He-3 Tubes	2.37E-02	3.2 E-3
Volumetric	-150	Channel 1 He-3 Tubes	4.27E-02	2.5 E-3
		Channel 2 He-3 Tubes	2.35E-02	3.3 E-3
		Channel 3 He-3 Tubes	8.89E-02	1.8 E-3
		Channel 4 He-3 Tubes	3.50E-02	2.3 E-3
		Channel 5 He-3 Tubes	3.50E-02	2.6 E-3
Volumetric	-100	Channel 1 He-3 Tubes	4.06E-02	2.5 E-3
		Channel 2 He-3 Tubes	2.73E-02	3.1 E-3
		Channel 3 He-3 Tubes	1.28E-01	1.5 E-3

Table 6.1 Continued

		Channel 4 He-3 Tubes	5.40E-02	1.8 E-3
		Channel 5 He-3 Tubes	5.09E-02	2.1 E-3
Volumetric	-50	Channel 1 He-3 Tubes	3.47E-02	2.7 E-3
		Channel 2 He-3 Tubes	3.38E-02	2.8 E-3
		Channel 3 He-3 Tubes	1.64E-01	1.3 E-3
		Channel 4 He-3 Tubes	7.41E-02	1.6 E-3
		Channel 5 He-3 Tubes	6.64E-02	1.9 E-3
Volumetric	50	Channel 1 He-3 Tubes	3.07E-02	2.9 E-3
		Channel 2 He-3 Tubes	3.97E-02	2.6 E-3
		Channel 3 He-3 Tubes	1.83E-01	1.2 E-3
		Channel 4 He-3 Tubes	8.69E-02	1.5 E-3
		Channel 5 He-3 Tubes	7.68E-02	1.7 E-3
Volumetric	100	Channel 1 He-3 Tubes	2.51E-02	3.2 E-3
		Channel 2 He-3 Tubes	3.36E-02	2.8 E-3
		Channel 3 He-3 Tubes	1.59E-01	1.3 E-3
		Channel 4 He-3 Tubes	7.53E-02	1.6 E-3

Table 6.1 Continued

		Channel 5 He-3 Tubes	6.74E-02	1.9 E-3
Volumetric	150	Channel 1 He-3 Tubes	1.85E-02	3.7 E-3
		Channel 2 He-3 Tubes	2.74E-02	3.1 E-3
		Channel 3 He-3 Tubes	1.26E-01	1.5 E-3
		Channel 4 He-3 Tubes	5.77E-02	1.8 E-3
		Channel 5 He-3 Tubes	5.34E-02	2.1 E-3
Volumetric	200	Channel 1 He-3 Tubes	1.28E-02	4.5 E-3
		Channel 2 He-3 Tubes	2.10E-02	3.5 E-3
		Channel 3 He-3 Tubes	9.01E-02	1.8 E-3
		Channel 4 He-3 Tubes	4.04E-02	2.1 E-3
		Channel 5 He-3 Tubes	3.89E-02	2.4 E-3

The results presented in Table 6.1 show that the errors are all within acceptable limits for both the surface and volumetric tallies performed. $R_{collided}$ term is then solved for using Equation 6.3 [13].

$$R_{Collided} = \frac{\sum_{i=1}^5 \sum_{g=1}^{30} q_{i,g} * S_g}{5.0} \quad \text{[Equation 6.3]}$$

Where $q_{i,g}$ is the incident Forward source in the i-th coarse mesh for energy group g, and S_g is the number of neutrons emitted per second into the energy group from the source (#/s) [13].

The $q_{i,g}$ is summed for the five detector faces, and the problem is then averaged over all 5 detector channel faces. Using Equations 6.3 and 6.2, we were able to generate a set of F_{factor} that are presented in Table 6.2.

Table 6.2: List of F-Factor values for the MCNP5 simulations at different intervals

Location	R_{collided}	$R_{\text{uncollided}}$	F_{factor}
X= -200	261	207	1.26E+00
X= -150	388	300	1.29E+00
X= -100	553	419	1.32E+00
X= -50	711	535	1.33E+00
X= 0	792	585	1.35E+00
X= 50	741	535	1.39E+00
X= 100	598	419	1.43E+00
X= 150	438	300	1.46E+00
X= 200	291	207	1.41E+00

Using the values presented in the Table 6.2. it should be possible to generate a number for R_{collided} at any of the different distance intervals considered in this work, given the initial source strength of an SNM [13]. This is tested using one of the already known sources: AmBe.

The F_{factor} is multiplied against the $R_{\text{uncollided}}$ for AmBe, which was found using Equation 6.1. The result of this equation is the $F_{\text{factor}} R_{\text{collided}}$, which was then compared to the Simulated R_{collided} which was calculated using a surface tally in MCNP5 for the AmBe source. The results of this test are presented in Table 6.3.

Table 6.3: R_{collided} , Calculated using F_{factor} compared to the R_{collided} calculated using simulation results.

$F_{\text{factor}} R_{\text{collided}}$	R_{collided} Calculated	R_{collided} calculated / F_{factor}
91659	93320	.9825

The results of Table 6.3 illustrate that the F_{factor} ratio can be used for various sources at any point in the FOV to quickly estimate R_{collided} . The minor difference between the two numbers

(less than 2%) can be explained as reasonable numerical differences in the manner of accomplishing the transport calculation. The F_{factor} relies on using scatter information for the same thirty group system, whereas the actual simulation uses scatter information as well as transport simulation to generate the final R_{collided} term [13].

6.3. Detector Response for Traveling SNM

The detector system response throughout the FOV varies in signal strength, as was seen in the F_{factor} calculation, and these same trends can also be seen in the actual simulation results from the 9 MCNP simulations that were performed. Figure 6.3 below shows these trends, the x axis represents the physical location of the source during that simulation for a vehicle traveling at 30 mph – within the FoV for 0.3s – and the y-axis represents the response – the error provided for the generation of this figure are presented in Table 6.1.

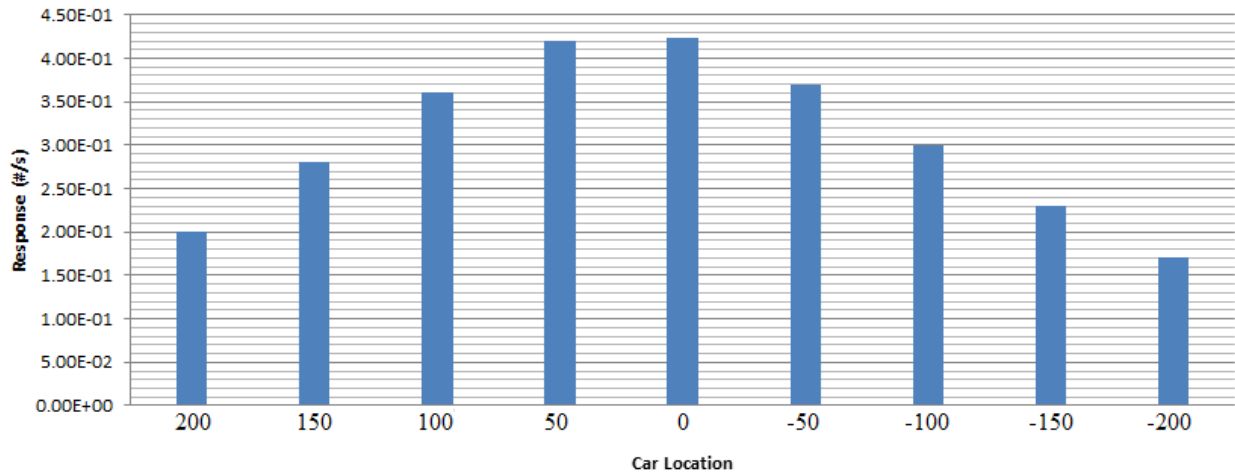


Figure 6.3: Response versus SNM location in detector FOV for a PuBe source with an initial strength of: 1.09E+06

Inspection of Figure 6.3 shows that the counts decrease the further the SNM gets from the zero reference position; however, the counts do not decrease symmetrically. The counts after the car has passed the detector – positive car location values – have a higher response than their negative distance counterparts. This is due to the scattering effects of the SNM interacting with

different internal major components of the car. When the car is approaching the detector source, its line of sight to the detector array is impeded by the car’s engine block (which is included in the model and consist of steel), and partially blocked by the gas tank (steel filled with gasoline). This physical barrier is not as present when the car has driven past the detector array, and therefore the counts registered in these intervals is slightly higher. This also explains why the F_{factors} , or ratios of “collided” to “uncollided” neutrons reported in Table 6.2 were not exactly symmetric around the center “zero” point – even when accounting for Monte Carlo statistical variations.

6.4. Minimum Number of Detectors

In order to determine the minimum numbers of detectors that will be required to establish a noise floor for this simulation, a background simulation must first be performed. This simulation was performed in MCNP5 using a background source painted across the top of the model – a 1 cm thick piece across the top of the model, stretching the models total x & y dimensions: -250x to 250x & -250y to 700y. The Background spectra used for the simulation is given below in Table 6.4a. The spectrum utilizes the 47 group library because the initial design of this emission spectra was with the 47 group library, and collapsing it further could result in unnecessary loss of detail. The source is the result of cosmic radiation, which is incident on all surfaces within the model, and set here to achieve a surface flux of 0.02 n/cm²/s at sea level. The Background simulation was performed successfully, and the results are displayed below in Table 6.4b.

Table 6.4a: Background Emission Spectra for a Background Source Using the 47 Group Library

Energy (MeV)	Probability
1.00E-07	8.49E-02
4.14E-07	5.70E-02
8.76E-07	2.85E-02
1.86E-06	2.68E-02
5.04E-06	3.69E-02
1.07E-05	3.02E-02
3.73E-05	4.79E-02
1.01E-04	3.90E-02
2.14E-04	2.84E-02

Table 6.4a Continued

4.54E-04	2.72E-02
1.58E-03	4.40E-02
3.35E-03	2.66E-02
7.10E-03	2.63E-02
1.50E-02	2.94E-02
2.19E-02	1.50E-02
2.42E-02	3.94E-03
2.61E-02	3.31E-03
3.18E-02	8.40E-03
4.09E-02	1.29E-02
6.74E-02	2.67E-02
1.11E-01	3.15E-02
1.83E-01	3.88E-02
2.97E-01	4.15E-02
3.69E-01	1.84E-02
4.98E-01	2.40E-02
6.08E-01	2.32E-02
7.43E-01	2.27E-02
8.21E-01	1.12E-02
1.00E+00	1.85E-02
1.35E+00	2.27E-02
1.65E+00	1.20E-02
1.92E+00	8.54E-03
2.23E+00	8.48E-03
2.35E+00	3.01E-03
2.37E+00	5.73E-04
2.47E+00	2.05E-03
2.73E+00	3.94E-03
3.01E+00	4.51E-03
3.68E+00	6.71E-03
4.97E+00	1.00E-02
6.07E+00	5.83E-03
7.41E+00	6.72E-03
8.61E+00	4.92E-03
1.00E+01	4.22E-03
1.22E+01	7.28E-03
1.42E+01	1.41E-02
1.73E+01	4.13E-02

Table 6.4b: Background Detector Response based on a mean surface neutron flux of 0.02 n/cm²/s

Background	Response [#s]	Rel Error
Channel 1 He-3 Tubes	9.26E-02	.0087
Channel 2 He-3 Tubes	1.88E-01	.0088
Channel 3 He-3 Tubes	3.72E+00	.0088
Channel 4 He-3 Tubes	8.14E+00	.0088
Channel 5 He-3 Tubes	5.39E+00	.0135
Total	1.75E+01	.0088

The detector response that was found from a background detector response can be used in all of the original tested sources – Cf, AmBe, and PuBe – because it is valid to assume that the fluence of neutrons can be added linearly. To establish a noise floor, the Currie Detection Limit formulation will be used. We wish to integrate a normalized Gaussian for 95% of its curve; this translates to a value of: $\pm 1.96\sigma$ from the central mean [14]. The source detection threshold is established by the Background response that was generated, and *the total counts that will be detected will be a summation of the Background and Source responses*. Assuming that the SNM response is weak – as is the case with the PuBe source – we know that the number of detected counts can be found by taking the total number of counts and subtracting the number of background counts. The error propagation that arises from this procedure in variance can be shown as [14]:

$$\sigma_d^2 = \sigma_T^2 + \sigma_b^2 \approx 2\sigma_b^2 \quad \text{[Equation 6.4]}$$

Letting $\sigma_b^2 = C_b * T_c$, Where C_b is the Background count rate (#/s), and T_c is the total counting time (s). Equation 6.4 can be rewritten as Equation 6.5 [14].

$$\sigma_d \approx \sqrt{2C_b T_c} \quad \text{[Equation 6.5]}$$

Figure 6.4 below depicts the Currie Limit (C_L), labeled in the figure as the Signal Decision Threshold Value. This value is established so that the minimum detectable activity for

the region outside the 1.96σ – or the probability of false alarm (PFA) – can be described by Equation 6.6 [14]:

$$C_L = 1.96\sqrt{2C_bT_c} \quad \text{[Equation 6.6]}$$

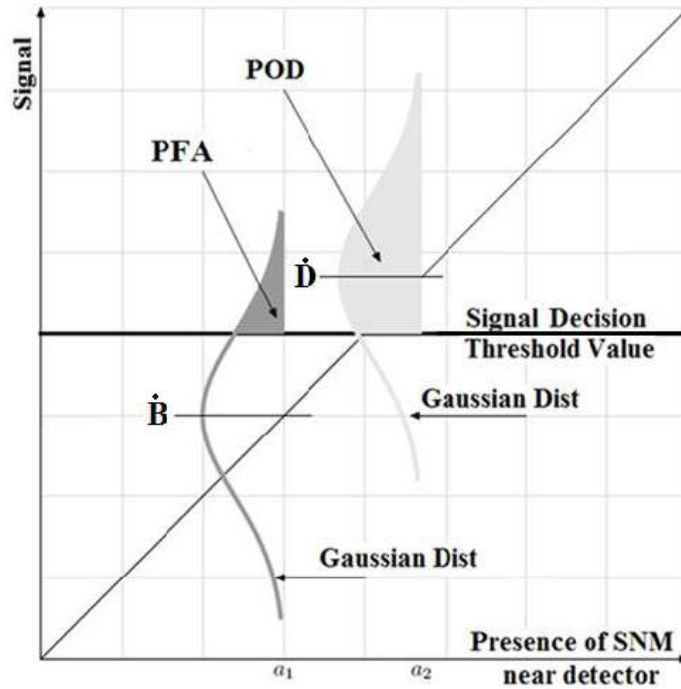


Figure 6.4: PFA and Currie Limit [14]

Assuming that real activity is present, the Real Activity Threshold counts are determined by Equation 6.7 [14]:

$$R_T = C_L + 1.96\sqrt{2C_bT_c + C_DT_c} \quad \text{[Equation 6.7]}$$

Where:

- R_T is the Real Activity Threshold Counts (#/s)
- C_L is Currie limit, count rate detector counts that are from background variance (#/s)
- C_b count rate from the Background (#/s)
- T_c is the total count time (s)
- C_D is the detector count rate for the source signal(#/s)

Substituting Equation 6.6 into Equation 6.7 we get Equation 6.8 [14].

$$R_T = 1.96\sqrt{2C_bT_c} + 1.96\sqrt{2C_bT_c + C_DT_c} \quad [\text{Equation 6.8}]$$

Letting the Real Activity Threshold Counts (R_T) be equal to the total count rate (C_D+C_b) multiplied by the total count time (T_c) Equation 6.8 can be rewritten as Equation 6.9 [13].

$$(C_b + C_D)T_c = 1.96\sqrt{2C_bT_c} + 1.96\sqrt{2C_bT_c + C_DT_c} \quad [\text{Equation 6.9}]$$

Knowing the average count rates for C_b and C_D , Equation 6.9 can be solved for T_c . Since equation 6.9 still contains the 1.96 values – the values that correspond to false alarm rate of 5% or less – solving this equation for T_c would give us the minimum counting time required for achieving a detection probability of 95% [14]. Since T_c is the total counting time accumulated over all detector assemblies, it can be rewritten as Equation 6.10 [13].

$$T_c = n_d T_R \quad [\text{Equation 6.10}]$$

Where n_d is the number of detector assemblies, and T_R is the real counting time for a single time gated detector assembly (s). An equation for determining the minimum number of detectors over the background can then be found using Equations 6.6 & 6.7.

$$n_{d,blocks} = \frac{(n_d - C_L)}{C_D T_R} \quad [\text{Equation 6.11}]$$

Isolating n_d in this expression would lead to an equation that describes the minimum number of detectors that are required for a false alarm probability of 5%. However, first values for T_p and T_r must be derived. Start by integrating Equation 6.1 over the time that the car is within the FOV, we can generate an expression for the total counts that can be detected. This integration is performed in Equation 6.12 [13].

$$\begin{aligned}
C_{g,uncollided} &= \int_{-\tau}^{\tau} dt R_g(x) \\
&= \int_{-\tau}^{\tau} dt \frac{S_g}{4\pi(z_0^2 + (v_0 t)^2)} \frac{(A_d \cdot z_0)}{(z_0^2 + (v_0 t)^2)^{1/2}} \quad [\text{Equation 6.12}]
\end{aligned}$$

Letting $\tau = \frac{L}{v_0}$, the time that is required for the car to pass half of the detectors FOV – i.e. from -200 cm to 0 cm, the evaluated, solved integral is shown in Equation 6.13 [13].

$$C_{g,uncollided} = \frac{S_g A_d}{2\pi z_0 v_0} \frac{L}{(z_0^2 + L^2)^{1/2}} = T_c C_p \quad [\text{Equation 6.13a}]$$

Or, in terms of the peak uncollided value C_p :

$$C_{g,uncollided} = \frac{S_g A_d}{4\pi z_0^2 v_0} \frac{2Lz_0}{(z_0^2 + L^2)^{1/2}} = (C_p) \cdot \frac{2Lz_0}{v_0(z_0^2 + L^2)^{1/2}} = T_c C_p \quad [\text{Equation 6.13b}]$$

Where T_c is the Effective Count Time (s), and C_p is the uncollided peak count rate (#/s) at $x=0$. Recalling that the peak count rate is at $x=0$ cm we can take the limit [13]:

$$C_p = \lim_{x \rightarrow 0} (R_g(x)) = \frac{(S_g)}{4\pi(z_0^2 + x^2)} \frac{(A_d \cdot z_0)}{(z_0^2 + x^2)^{1/2}} = \frac{S_g A_d}{4\pi z_0^2} \quad [\text{Equation 6.14}]$$

Using this we can solve for the “effective” counting time: T_p . This is shown below in Equation 6.15 [13].

$$T_p = \frac{2Lz_0}{v_0(z_0^2 + L^2)^{1/2}} = T_r \frac{z_0}{(z_0^2 + L^2)^{1/2}} = T_r \cos \theta \quad [\text{Equation 6.15}]$$

Where T_r is the real counting time (s) and is equal to: $\frac{2L}{v_0}$. The final form of Equation 6.15 is a more simplified representation for the time period when the SNM is within the FoV of the detector array. Two values for T_r can be determined at the two different speeds that are being

considered for the SNM as it passes through the FOV: 30 mph and 60 mph. The effective times for 30 and 60 mph are shown below in Equations 6.18 *a* and *b* respectively [13].

$$T_r = \frac{2L}{v_0} \approx 0.30s \quad \text{[Equation 6.18a]}$$

$$T_r = \frac{2L}{v_0} \approx 0.15s \quad \text{[Equation 6.18b]}$$

Using the values obtained for T_r at 30 and 60 mph, we can solve equation 6.16, and get the two corresponding values for T_p . This is achieved in Equations 6.19 *a* and *b* [13].

At 30:

$$T_p = T_r \cos \theta = 0.30 \cdot \cos(45^\circ) = 0.2109 s \quad \text{[Equation 6.19a]}$$

At 60:

$$T_p = T_r \cos \theta = 0.15 \cdot \cos(45^\circ) = 0.106 s \quad \text{[Equation 6.19b]}$$

The two T_r values are considered constants for the two trial cases that are being considered: 30, and 60 mph. The corresponding values for T_p are also considered to be constants for the speeds considered, and as long as the detector FOV is aliased to a forty-five degree angle determined from a 200 cm FoV. Knowing the net source emission rate, we can determine the minimum number of detectors that would be required for TSADS system to differentiate a signal from background to SNM. This is shown below in Table 6.5 for each of the four SNM tested in MCNP.

Table 6.5: Number of detectors needed for each channel type to distinguish SNM from Background for a Pu-Be, Am-Be, Cf, and 14MeV source at 30 mph

SNM Type	Channel 1	Channel 2	Channel 3	Channel 4	Channel 5
Pu-Be	61	68	63	198	183
Am-Be	3	2	1	2	2
Cf-252	1	1	1	1	1
14MeV	2	3	5	7	6
8kg WGPu	1	1	1	1	1

The Pu-Be source requires the greatest number of detectors in order to distinguish the SNM from the background signal. This is expected due to the low response of Pu-Be versus the relatively higher response of the background count. The Cf-252 and 8 kg Pu sphere each requires the fewest number of detectors. This can be attributed to the relatively large number of counts generated by these sources when compared to the background count rates. This table shows that in order to confirm the presence of an SNM for a weakly emitting source, multiple detector assemblies are needed.

7. CONCLUSION

7.1. Summary of Work

A full overview of the work completed on the detector system shows that the system is reliable, and can be used in realistic environments. Chapter's 2 and 3 showed that PENTRAN could be used to create an accurate model that can successfully simulate both Forward and Adjoint transport using 3-D deterministic modeling. The results of which could be coupled, within 90.00% accuracy. Chapter 4 used the Adjoint results that were presented in Chapter 3 to verify that the detector channels were operating as they had been designed; only detecting particles within certain energy ranges. Chapter 5 demonstrated that by using the Adjoint currents obtained in Chapter 3, a Forward source could be coupled with this information to give an accurate response for each detector channel. These channel responses could then be used in a relative ratio method to distinguish between sources by identifying different characteristics of their emission spectra. This work completed goal (ii). Chapter 6 discussed how SNM could be detected at various speeds: 30 & 60 mph. However, in order to be able to detect the SNM, and differentiate it from background noise, a large number of detector arrays are needed. This could become a possible hurdle for implementation, because of the cost of building and maintaining a large number of units, and also because of the large space that would be needed to accommodate the system. This work accomplished goal (i). With these two goals accomplished, a detector array has been successfully designed that can: determine the presence of an SNM in a passing vehicle at various highway speeds, and determine the general shape of the emission spectra for that SNM.

7.2. Future Work

To move into the phase of work, a real model would need to be constructed to verify the detection capabilities of the five detector channel designs. Once this was accomplished, the full model could be tested against a variety of SNM sources to verify the findings in Chapter 5, and possibly expand on the number/types of sources tested. Finally, the model would need to be tested in a real world setting, using a lab controlled SNM drive by.

APPENDIX A-1

REACT CODE

```
!  
! Adjoint Reaction Rate Calculator  
!  
! by Scottie Walker  
! Michael Chin (May 2012)  
! Matthew Molinar (May 2012)  
  
! Version 1.3  
!  
! This code is used to process the flux files from adjoint PENTRAN  
! runs to calculate reaction rates and various other quantities.  
!  
!-----  
!  
! PROGRAM AREACT  
!  
! IMPLICIT REAL (A-H,O-Z)  
! IMPLICIT INTEGER (I-N)  
!  
! MAIN PROGRAM  
!  
!/////////  
!  
! CALL IHEADR  
! CALL INSIFT  
!  
! STOP  
!  
! END  
!  
!-----  
!  
! SUB IHEADR  
!  
! PURPOSE OF IHEADR ROUTINE:  
! -To print header when program is initiated  
!  
! NOTES:  
! -None  
!  
! AUTHOR (date):  
! S. W. Walker (January 2012)
```

```

!
! WITH CONTRIBUTIONS FROM:
! M. Chin (May 2012)
! M. Molinar (May 2012)
!
SUBROUTINE IHEADR
!
WRITE(*,'(A2//) ')
WRITE(*,'(2X,A46)')'Adjoint Reaction Rate Evaluation Program '
WRITE(*,'(A2)')
WRITE(*,'(2X,A48)')   Version 1.3 DOUBLE PRECISION
WRITE(*,'(A2)')
WRITE(*,'(2X,A48)')   Scottie W. Walker
WRITE(*,'(2X,A48)')   Michael R. Chin
WRITE(*,'(2X,A48)')   Matthew P. Molinar
WRITE(*,*)
WRITE(*,'(2X,A48)')   May 2012
WRITE(*,'(A2)')
!
END
!
! *****
! SUB INSIFT
! *****
! PURPOSE OF INSIFT ROUTINE:
! -To read and process data
!
SUBROUTINE INSIFT
!
IMPLICIT REAL (A-H,O-Z)
IMPLICIT INTEGER (I-N)
!
REAL, DIMENSION(150) :: tstnum, grpegy, src
!
REAL, DIMENSION(1500) :: dx,dy,dz,vol,rr,spacflx
INTEGER, DIMENSION(1500) :: icm
!
CHARACTER(10) :: matname
CHARACTER(64) :: datfnam, outfnam, dxdydzf, rrxsecf, flxlogf, flxlogg, srcf
CHARACTER(80) :: dummy
! Add in .xs naming support - MC
CHARACTER(80) :: xsname
! Generalization of energy group structure from flx.Log file - MC
INTEGER :: ingrp
!

```

```

LOGICAL exists, open
!
! Set Data Index params:
! DataColumns, GlobalCoarseCells, CMdataindex, Targdataindex, Fluxindex, etc
!     Forward source that was flipped for the
!     adjoint calculation.
! Note: The forward source for the adjoint case is the
! normalized cell volumetric source density term in n/(cm^3*s). MC
!
! *****
! Information location:
! *****
! Total number of ASCII Columns in data files
ntdat=7
!
!     Coarse mesh Column Index
icmidx=2
!
! Target Material Column Index
itargm=3
!
! Flux Column Index
iflux=7
!
! Material to Sum Rxns
!
! *****
! Files Needed:
! *****
!     response xsecs for neutron/gamma response xsec
!     dxdydz.out for Coarse mesh data -> Volume
!     flx.Log to list group data files in a listing
!     group files named in flx.Log
!     energy.adj for flipped energy group upper bounds (MeV)
!     source.fwd for flipped source terms (normalized to 1).
!
! *****
! Input information:
! *****
!     Each of the read (*,*) statements require an input
!
! WRITE(*,'(A40)') Input Material # to sum reactions for: '
! READ(*,*) nmat
!
!
! WRITE(*,'(A22)') Input Material Name: '

```

```

READ(*,*) matname
!
! Generalized support for arbitrary number of groups
WRITE(*,'(A24)') Input Number of Groups: '
READ(*,*) ingrp
!
! Initalize arrays before filling them
DO j=1, ingrp
  grpegy(j) = 0.0
  src(j) = 0.0
END DO
!
! Prompt for number of coarse meshes (technically this is in dxdydz)
WRITE(*,'(A31)') Input Number of Coarse Meshes: '
READ(*,*) ntgcm
!
! Generalized support for different cross section files - MC
WRITE(*,'(A35)') Input Cross Section Filename (.xs): '
READ(*,*) xsname
!
! Arbitrary Energy Group Selection
! Increment our file counter j after initalizing it to zero
j = 0
!
OPEN(17, FILE='energy.fwd', ACCESS='SEQUENTIAL')
  j = j + 1
  DO j = 1, ingrp
    READ(17,*) grpegy(j)
  END DO
CLOSE(17)
!
! Arbitrary Source Selection
! Increment our file counter j after initalizing it to zero
!
! Echo our energy.dat and source.dat to the screen for reference
DO j=1, ingrp
  WRITE(*,*) "egybnd(", j, "): ", grpegy(j)
END DO
!
WRITE(*,*)
!
! *****
! Initialize problem: averages, fluxsums, responses, group count
! *****
!
sigavg=0

```

```

flxsum=0
respons=0
rr=0
igrpcent=0
xavgmax=0
favgmax=0
eavgmax=0
!
! *****
! Read dxdydz file and compute volume
! *****
! Note: This dxdydz term is the volume of the forward source term!
! When EOF is reached, control transfers to statement 150
! and continues from there.
!
      dxdydzf='dxdydz.out'
      OPEN (3, FILE=dxdydzf, ACCESS='SEQUENTIAL')
      i=0
      READ (3,'(A)') dummy
      WRITE(*,'(A80)') dummy
100  i=i+1
      READ (3,*,END=150) icm(i), dx(i), dy(i), dz(i)
      WRITE(*,'(I5,3(2X,F8.3))') icm(i), dx(i), dy(i), dz(i)
      vol(i)=dx(i)*dy(i)*dz(i)
      GOTO 100
150  i=i-1
      IF(i.NE.ntgcm)THEN
        WRITE(*,*)'ERROR: Cell count i ',i,' mismatch ntgcm ', ntgcm
        STOP
      END IF
      WRITE(*,*)' Read ',i,' Cell Dimensions '
      WRITE(*,*) ''
      CLOSE(3)
!
! -----
! Read Response Cross section file header from device 1 and
! the flx.log header from device 2.
!
! The two read statements read and write the data of the first
! two lines in the cross section file to the variable dummy
! (not needed). The data actually begins on the 3rd line.
!
! The first line of the flx.log is a header and the single
! read/write statement puts that information into dummy.
!

```

```

!       Both of these files remain open until the very end of the
!       program.
! -----
!
! *****
! Read cross section input file and flx.Log file
! *****
rrxsecf = xsname
! Changed to general filename - MC
OPEN (1, FILE = rrxsecf, ACCESS = 'SEQUENTIAL')
READ (1,'(A)') dummy
WRITE(*,'(A80)') dummy
READ (1,'(A)') dummy
WRITE(*,'(A80)') dummy
!
! Read flux datafile listing from device 2
!
flxlogf = 'flx.Log'
OPEN (2, FILE = flxlogf, ACCESS='SEQUENTIAL')
READ (2,'(A)') dummy
WRITE(*,'(A80)') dummy
!
! *****
! Open output file
! *****
!       The write statements are directed toward device #11, which is the
!       shorthand of the output file. The information mentioned is written to
!       the output file alone and does not appear on the screen.
!
itest=INDEX(matname,' ')-1
IF(itest.LE.10) THEN
  outfnam=matname(1:itest)//'-frx.out'
ELSE
  outfnam=matname(1:10)//'-frx.out'
END IF
OPEN (11, FILE=outfnam, ACCESS='SEQUENTIAL')
WRITE(11,*) ' ,outfnam
WRITE(11,*)'-----'
WRITE(11,*)' READ Data from the Following Files : '
WRITE(11,'(A31,A30)')      dxdydz mesh data... ' ,dxdydzf
WRITE(11,'(A31,A30)')      reaction rate xs data... ' ,rrxsecf
WRITE(11,'(A31,A30)')      flux log filename list... ' ,flxlogf
WRITE(11,'(A31,A40)')      forward energy list... energy.fwd'
WRITE(11,*)'-----'
!
! *****

```



```

!          -----BEGIN GROUP DEPENDENT SEQUENCE-----
!          ****
200 CONTINUE
!
!   Increment group counter, reset material counter, target matl volume
!       igrpct was previously set to 0.
!
!   igrpct=igrpct+1
!   imatcnt=0
!   voltarg=0
!
!   Initialize fluxmax and material bdy offsets
!
!   fluxmax=0
!   xmaxoff=3.0
!   ymaxoff=0
!   zmaxoff=0
!   xmax=0
!   ymax=0
!   zmax=0
!
!   rmfpa=0.0
!
!   Write Group and Read Group Response Cross Section
!       Device #1 is the cross section file and the header has already
!       been dumped, so the next line begins with the absorption
!       cross section, which is conveniently the first value!
!   IF (igrpct .LE. ingrp) THEN
!       WRITE(*,*)' Group Counter = ', igrpct, ' Out of ', ingrp,
& ' Groups.'
!       READ (1,*) sigabs
!       WRITE(*,*) ' siga = ',sigabs
!       IF(sigabs.GT.1E-10)THEN
!           rmfpa = 1/sigabs
!       END IF
!   ELSE
!       igrpct=igrpct-1
!   END IF
!
!   Get flux datafile assignment data
!
!       Device #2 is the flx.log and the first flux log value is assigned
!       to datfnam (e.g. polyj201.flx).
!
!       The header information was already dumped to dummy above, so the
!       desired flux file names begin to be read on line 250.

```

```

!
250  CONTINUE
      READ (2,*,END=400) datfnam
!
!   Open flux datafile and read vectors of flux data
!
!   The flux files are opened below and the read statement dumps
!       the header information to dummy.  The write statement lists
!       the name of the flux file and the read statement on line 350
!       begins to pull out the necessary data.
!
      OPEN (10, FILE = datfnam, ACCESS='SEQUENTIAL')
      READ (10,'(A)') dummy
      WRITE(*,*) 'Read data from : ', datfnam
300  CONTINUE
      READ (10,*,END=350) (tstnum(iety), iety=1,ntdat)
!
!           The read statements above read information from: 1) columns
!           1 - 7 of the flux file datfnam and 2) the forward source file.
!           When the EOF is reached, control goes to line 350.
!
!   If target material compute response from that cell
!
      IF (INT(tstnum(itargm)).EQ.nmat) THEN
          imatcnt=imatcnt+1
          itstcm=INT(tstnum(icmidx))
          sigavg = sigavg + (tstnum(iflux) * sigabs * vol(itstcm))
          flxsum = flxsum + (tstnum(iflux) * vol(itstcm))
          fluxmaxold = fluxmax
          fluxmax=MAX(fluxmax, tstnum(iflux))
          IF(fluxmax.NE.fluxmaxold)THEN
              xmax=tstnum(iflux-3) - xmaxoff
              ymax=tstnum(iflux-2) - ymaxoff
              zmax=tstnum(iflux-1) - zmaxoff
          END IF
!
          rr(igrpct)=rr(igrpct) +
&           (tstnum(iflux) * sigabs * vol(itstcm))
          respons=respons+(tstnum(iflux) * sigabs * vol(itstcm))
              ! Add in spatially averaged flux values over all meshes
          spacflx(igrpct)=flxsum/imatcnt
          END IF
          GOTO 300
!
!   Summary of Group findings
!

```

```

350 CONTINUE
!
CLOSE(10)
voltarg=imatcnt*vol(itstcm)
!
!
WRITE(*,*) ' Found ',imatcnt,' matl# ',nmat,
& ' meshes covering ', voltarg,' cm3 '
WRITE(*,'(A5,I3,A1,1PE10.3,A5,A12,1PE13.6,A10,
& 0PF6.2,A1,0PF6.2,A1,0PF6.2,A2,1PE13.6)')
& ' Grp ',igrpcent,' ',grpegy(igrpcent),' MeV ',' #/s : ',
& rr(igrpcent),' MaxFlux (' ,xmax,',',ymax,',',zmax,')=' ,fluxmax
WRITE(*,*) '
!
IF(igrpcent.EQ.1)THEN
WRITE(11,*) ' Found ',imatcnt,' matl# ',nmat,
& ' meshes covering ', voltarg,' cm3'
END IF
WRITE(11,'(A5,I3,A1,1PE10.3,A5,A12,1PE13.6,A10,
& 0PF6.2,A1,0PF6.2,A1,0PF6.2,A2,1PE13.6)')
& ' Grp ',igrpcent,' ',grpegy(igrpcent),' MeV ',' #/s : ',
& rr(igrpcent),' MaxFlux (' ,xmax,',',ymax,',',zmax,')=' ,fluxmax
!
! Compute Response-Weighted xmax, flux, and energy
!
xavgmx=xavgmx + (xmax*rr(igrpcent))
favgmx=favgmx + (fluxmax*rr(igrpcent))
eavgmx=eavgmx + (grpegy(igrpcent)*rr(igrpcent))
!
!           igrpneut = 47 from before, which is = igrpmax as well.
!
!
IF(igrpcent.EQ.igrpneut)THEN
IF(igrpcent .EQ. ingrp) THEN
GOTO 400
END IF
GOTO 200
!
!           GOTO 200 sends us to increment the group counter and to get
!           the next neutron group.
!
400 CONTINUE
!
! Report Results
!
!
xavgmx = xavgmx/respons

```

```

    favgmx = favgmx/respons
    eavgmx = eavgmx/respons
1000 FORMAT(A28,I3,A9,1PE13.6,A7,1PE13.6,A13)
!

    WRITE(11,*) ' -- Summary for ',matname,' --'
    WRITE(11,*) ''
    WRITE(11,1000)' Total Neutron Response from ', ingrp,
& ' Groups: ', respons,' cts/s metric:'
    WRITE(11,*) ' Avg g Resp-Weighted xmax ',xavgmx,' cm '
    WRITE(11,*) ' Avg g Resp-Weighted flux ',favgmx ,' n/cm2/s '
    WRITE(11,*) ' Avg g Resp-Weighted energy ',eavgmx ,' MeV '
    WRITE(11,*) ''
    WRITE(11,*)' --- End of Data for ',matname,' ---'
    WRITE(11,*) ''
    IF (igrpcent .LT. ingrp) THEN
        rr=0
        flxsum=0
        respons=0
        xavgmx=0
        GOTO 200
    END IF
!
    CLOSE(2)
    CLOSE(1)
    CLOSE(11)
!
    STOP
!
    END

```

**APPENDIX A-2
AREACT CODE**

```
!  
! Adjoint Reaction Rate Calculator  
!  
! by Scottie Walker  
! Michael Chin (May 2012)  
! Matthew Molinar (May 2012)  
  
! Version 1.3  
!  
! This code is used to process the flux files from adjoint PENTRAN  
! runs to calculate reaction rates and various other quantities.  
!  
!-----  
!  
! PROGRAM AREACT  
!  
! IMPLICIT REAL (A-H,O-Z)  
! IMPLICIT INTEGER (I-N)  
!  
! MAIN PROGRAM  
!  
!/////////  
!  
! CALL IHEADR  
! CALL INSIFT  
!  
! STOP  
!  
! END  
!  
!-----  
!  
! SUB IHEADR  
!  
! PURPOSE OF IHEADR ROUTINE:  
! -To print header when program is initiated  
!  
! NOTES:  
! -None  
!  
! AUTHOR (date):  
! S. W. Walker (January 2012)  
!
```

```

! WITH CONTRIBUTIONS FROM:
! M. Chin (May 2012)
! M. Molinar (May 2012)
!
SUBROUTINE IHEADR
!
WRITE(*,'(A2///) ')
WRITE(*,'(2X,A46)') Adjoint Reaction Rate Evaluation Program
WRITE(*,'(A2)')
WRITE(*,'(2X,A48)') Version 1.3 DOUBLE PRECISION
WRITE(*,'(A2)')
WRITE(*,'(2X,A48)') Scottie W. Walker
WRITE(*,'(2X,A48)') Michael R. Chin
WRITE(*,'(2X,A48)') Matthew P. Molinar
WRITE(*,*)
WRITE(*,'(2X,A48)') May 2012
WRITE(*,'(A2)')
!
END
!
! *****
! SUB INSIFT
! *****
! PURPOSE OF INSIFT ROUTINE:
! -To read and process data
!
SUBROUTINE INSIFT
!
IMPLICIT REAL (A-H,O-Z)
IMPLICIT INTEGER (I-N)
!
REAL, DIMENSION(150) :: tstnum, grpegy, src
!
REAL, DIMENSION(1500) :: dx,dy,dz,vol,rr,spacflx
INTEGER, DIMENSION(1500) :: icm
!
CHARACTER(10) :: matname
CHARACTER(64) :: datfnam, outfnam, dxdydzf, flxlogf, flxlogg, srcf
CHARACTER(80) :: dummy
! Generalization of energy group structure from flx.Log file - MC
INTEGER :: ingrp
!
LOGICAL exists, opend
!
! Set Data Index params:

```

```

! DataColumns, GlobalCoarseCells, CMdataindex, Targdataindex, Fluxindex, etc
!   Forward source that was flipped for the
!   adjoint calculation.
! Note: The forward source for the adjoint case is the
! normalized cell volumetric source density term in n/(cm^3*s). MC
!
! *****
! Information location:
! *****
! Total number of ASCII Columns in data files
ntdat=7
!
!   Coarse mesh Column Index
icmidx=2
!
! Target Material Column Index
itargm=3
!
! Flux Column Index
iflux=7
!
! Material to Sum Rxns
!
! *****
! Files Needed:
! *****
!   response xsecs for neutron/gamma response xsec
!   dxdydz.out for Coarse mesh data -> Volume
!   flx.Log to list group data files in a listing
!   group files named in flx.Log
!   energy.adj for flipped energy group upper bounds (MeV)
!   source.fwd for flipped source terms (normalized to 1).
!
! *****
! Input information:
! *****
!   Each of the read (*,*) statements require an input
!
! WRITE(*,'(A40)') Input Material # to sum reactions for: '
! READ(*,*) nmat
!
!
! WRITE(*,'(A22)') Input Material Name: '
! READ(*,*) matname
!
! Generalized support for arbitrary number of groups

```

```

WRITE(*,'(A24)') Input Number of Groups: '
READ(*,*) ingrp
!
! Initialize arrays before filling them
DO j=1, ingrp
    grpegy(j) = 0.0
    src(j) = 0.0
END DO
!
! Prompt for number of coarse meshes (technically this is in dxdydz)
WRITE(*,'(A31)') Input Number of Coarse Meshes: '
READ(*,*) ntgcm
!
! Arbitrary Energy Group Selection
! Increment our file counter j after initializing it to zero
j = 0
!
OPEN(17, FILE='energy.adj', ACCESS='SEQUENTIAL')
    j = j + 1
    DO j = 1, ingrp
        READ(17,*) grpegy(j)
    END DO
CLOSE(17)
!
! Arbitrary Source Selection
! Increment our file counter j after initializing it to zero
!
OPEN(18, FILE='source.adj', ACCESS='SEQUENTIAL')
    j = j + 1
    DO j = 1, ingrp
        READ(18,*) src(j)
    END DO
CLOSE(18)
!
! Echo our energy.dat and source.dat to the screen for reference
DO j=1, ingrp
    WRITE(*,*) "egyband(", j, "): ", grpegy(j)
END DO
!
WRITE(*,*)
!
DO j=1, ingrp
    WRITE(*,*) "src(", j, "): ", src(j)
END DO
!
WRITE(*,*)

```



```

!
! *****
! Initialize problem: averages, fluxsums, responses, group count
! *****
!
!
!   flxsum=0
!   respons=0
!   rr=0
!   igrpct=0
!   xavgmax=0
!   favgmax=0
!   eavgmax=0
!
! *****
! Read dxdydz file and compute volume
! *****
! Note: This dxdydz term is the volume of the forward source term!
! When EOF is reached, control transfers to statement 150
! and continues from there.
!
!       dxdydzf='dxdydz.out'
!       OPEN (3, FILE=dxdydzf, ACCESS='SEQUENTIAL')
!       i=0
!       READ (3,'(A)') dummy
!       WRITE(*,'(A80)') dummy
100  i=i+1
!       READ (3,*,END=150) icm(i), dx(i), dy(i), dz(i)
!       WRITE(*,'(I5,3(2X,F8.3))') icm(i), dx(i), dy(i), dz(i)
!       vol(i)=dx(i)*dy(i)*dz(i)
!       GOTO 100
150  i=i-1
!       IF(i.NE.ntgcm)THEN
!         WRITE(*,*)'ERROR: Cell count i ',i,' mismatch ntgcm ', ntgcm
!         STOP
!       END IF
!       WRITE(*,*)' Read ',i,' Cell Dimensions '
!       WRITE(*,*)' '
!       CLOSE(3)
!
! -----
!
! Read Response Cross section file header from device 1 and
! the flx.log header from device 2.
!
! The two read statements read and write the data of the first
! two lines in the cross section file to the variable dummy

```

```

!      (not needed). The data actually begins on the 3rd line.
!
!      The first line of the flx.log is a header and the single
!      read/write statement puts that information into dummy.
!
!      Both of these files remain open until the very end of the
!      program.
!
!      -----
!
!      *****
!      Read cross section input file and flx.Log file
!      *****

!      Changed to general filename - MC
!
!      Read flux datafile listing from device 2
!
!      flxlogf = 'flx.Log'
!      OPEN (2, FILE = flxlogf, ACCESS='SEQUENTIAL')
!      READ (2,'(A)') dummy
!      WRITE(*,'(A80)') dummy
!
!      *****
!      Open output file
!      *****
!
!      The write statements are directed toward device #11, which is the
!      shorthand of the output file. The information mentioned is written to
!      the output file alone and does not appear on the screen.
!
!      itest=INDEX(matname,' ')-1
!      IF(itest.LE.10) THEN
!         outfnam=matname(1:itest)//'-arx.out'
!      ELSE
!         outfnam=matname(1:10)//'-arx.out'
!      END IF
!      OPEN (11, FILE=outfnam, ACCESS='SEQUENTIAL')
!      WRITE(11,*)' ',outfnam
!      WRITE(11,*)'-----'
!      WRITE(11,*)' READ Data from the Following Files : '
!      WRITE(11,'(A31,A30)')'      dxdydz mesh data... ',dxdydzf
!      WRITE(11,'(A31,A30)')' flux log filename list... ',flxlogf
!         WRITE(11,'(A45)')'      adjoint energy list... energy.adj'
!         WRITE(11,'(A45)')'      adjoint source list... source.adj'
!      WRITE(11,*)'-----'
!
!      *****

```

```

!           -----BEGIN GROUP DEPENDENT SEQUENCE-----
!           ****
200  CONTINUE
!
!   Increment group counter, reset material counter, target matl volume
!       igrpct was previously set to 0.
!
!   igrpct=igrpct+1
!   imatcnt=0
!   voltarg=0
!
!   Initialize fluxmax and material bdy offsets
!
!   fluxmax=0
!   xmaxoff=3.0
!   ymaxoff=0
!   zmaxoff=0
!   xmax=0
!   ymax=0
!   zmax=0
!
!   rmfpa=0.0
!
!   Write Group and Read Group Response Cross Section
!       Device #1 is the cross section file and the header has already
!       been dumped, so the next line begins with the absorption
!       cross section, which is conveniently the first value!
!
!
!   Get flux datafile assignment data
!
!       Device #2 is the flx.log and the first flux log value is assigned
!       to datfnam (e.g. polyj201.flx).
!
!       The header information was already dumped to dummy above, so the
!       desired flux file names begin to be read on line 250.
!
250  CONTINUE
!       READ (2,*,END=400) datfnam
!
!   Open flux datafile and read vectors of flux data
!
!   The flux files are opened below and the read statement dumps
!   the header information to dummy. The write statement lists
!   the name of the flux file and the read statement on line 350
!   begins to pull out the necessary data.

```

```

!
OPEN (10, FILE = datfnam, ACCESS='SEQUENTIAL')
READ (10,'(A)') dummy
WRITE(*,*) 'Read data from : ', datfnam
300  CONTINUE
    READ (10,*,END=350) (tstnum(iety), iety=1,ntdat)
!
!           The read statements above read information from: 1) columns
!           1 - 7 of the flux file datfnam and 2) the forward source file.
!           When the EOF is reached, control goes to line 350.
!
! If target material compute response from that cell
!
IF (INT(tstnum(itargm)).EQ.nmat) THEN
    imatcnt=imatcnt+1
    itstcm=INT(tstnum(icmidx))
!
    fluxmaxold = fluxmax
    fluxmax=MAX(fluxmax, tstnum(iflux))
    IF(fluxmax.NE.fluxmaxold)THEN
        xmax=tstnum(iflux-3) - xmaxoff
        ymax=tstnum(iflux-2) - ymaxoff
        zmax=tstnum(iflux-1) - zmaxoff
    END IF
!
    rr(igrpct)=rr(igrpct) +
&      (tstnum(iflux) * src(igrpct) * vol(itstcm))
    respons=respons+(tstnum(iflux) * src(igrpct) * vol(itstcm))
        ! Add in spatially averaged flux values over all meshes
    spacflx(igrpct)=flxsum/imatcnt
    END IF
    GOTO 300
!
! Summary of Group findings
!
350  CONTINUE
!
    CLOSE(10)
    voltarg=imatcnt*vol(itstcm)
!
!
    WRITE(*,*) ' Found ',imatcnt,' matl# ',nmat,
& ' meshes covering ', voltarg,' cm3 '
    WRITE(*,'(A5,I3,A1,1PE10.3,A5,A12,1PE13.6,A10,
& 0PF6.2,A1,0PF6.2,A1,0PF6.2,A2,1PE13.6)')
& ' Grp ',igrpct,' ',grpegy(igrpct),' MeV ', ' abs #/s : ',

```

```

& rr(igrpcent),' MaxFlux (' ,xmax,',',ymax,',',zmax,')=',fluxmax
WRITE(*,*)' '
!
IF(igrpcent.EQ.1)THEN
WRITE(11,*) ' Found ',imatcnt,' matl# ',nmat,
& ' meshes covering ', voltarg,' cm3'
END IF
WRITE(11,('(A5,I3,A1,1PE10.3,A5,A12,1PE13.6,A10,
& 0PF6.2,A1,0PF6.2,A1,0PF6.2,A2,1PE13.6)')
& ' Grp ',igrpcent,' ',grpegy(igrpcent),' MeV ', '#/s : ',
& rr(igrpcent),' MaxFlux (' ,xmax,',',ymax,',',zmax,')=',fluxmax
!
! Compute Response-Weighted xmax, flux, and energy
!
xavgmx=xavgmx + (xmax*rr(igrpcent))
favgmx=favgmx + (fluxmax*rr(igrpcent))
eavgmx=eavgmx + (grpegy(igrpcent)*rr(igrpcent))
!
!          igrpneut = 47 from before, which is = igrpmax as well.
!
! IF(igrpcent.EQ.igrpneut)THEN
IF(igrpcent .EQ. ingrp) THEN
GOTO 400
END IF
GOTO 200
!
!          GOTO 200 sends us to increment the group counter and to get
!          the next neutron group.
!
400 CONTINUE
!
! Report Results
!
!
xavgmx = xavgmx/respons
favgmx = favgm/respons
eavgmx = eavgmx/respons
1000 FORMAT(A28,I3,A9,1PE13.6,A7,1PE13.6,A13)
!
WRITE(11,*) ' -- Summary for ',matname,' --'
WRITE(11,*) ' '
WRITE(11,1000)' Total Neutron Response from ', ingrp,
& ' Groups: ', respons,' cts/s metric:'
WRITE(11,*) ' Avg g Resp-Weighted xmax ',xavgmx,' cm '
WRITE(11,*) ' Avg g Resp-Weighted flux ',favgmx , ' n/cm2/s '

```

```
WRITE(11,*) ' Avg g Resp-Weighted energy ',eavgmx ,' MeV '  
WRITE(11,*) ' '  
WRITE(11,*) ' --- End of Data for ',matname,' ---'  
WRITE(11,*) ' '  
IF (igrpct .LT. ingrp) THEN  
  rr=0  
  flxsum=0  
  respons=0  
  xavgmx=0  
  GOTO 200  
END IF  
!  
CLOSE(2)  
CLOSE(1)  
CLOSE(11)  
!  
STOP  
!  
END
```

REFERENCES

1. Ianakiev, Kiril, and Martyn Swinhoe. *A Modular Neutron Detector*. Los Alamos National Laboratory, Web. 9 May 2013. <http://www.lanl.gov/quarterly/q_sum03/neutron_detect.shtml>.
2. Krane, Kenneth S. *Introductory Nuclear Physics*. 2ndnd ed. Hoboken: John Wiley & Sons inc., 1988. 452-53. Print.
3. Ghita, Gabriel; Sjoden, Glenn; Baciak, James. "A Methodology for Experiment and 3-D Computational Radiation Transport Assessments of Pu-Be Neutron Sources" *Nuclear Technology*, **159**, pp.319-331 (2007).
4. G. Sjoden and A. Haghigat, "PENTRAN - A 3-D Cartesian Parallel SN Code with Angular, Energy, and Spatial Decomposition", *Proceedings of the Joint International Conference on Mathematical Methods and Supercomputing for Nuclear Applications*, p. 553, Saratoga Springs, NY (1997).
5. Sjoden, Glenn E. "PENTRAN Code System Users Guide." *HSW Technology*. Nov. 2008. Web. 9 May 2013. <<http://www.hswtech.com/pdfs/PENTRANmanual.pdf>>. p.14
6. Los Alamos National Laboratory. MCNP code description. <http://mcnp.lanl.gov/>
7. Sjoden, Glenn E. "Deterministic Adjoint Transport Applications for He-3 Neutron Detector Design" *annals of Nuclear Energy*, **29**, pp.1055-1071 (2002).
8. Sjoden, Glenn E., and Ce Yi. *Transport Simulation and Validation of a Synthetic Aperture SNM Detection System ("T-SADS")*. Quarterly Report July 2012. Print.
9. Rinard, P. "Neutron Interactions with Matter." *Federation of American Scientists*. Web. 9 May 2013. <<http://www.fas.org/sgp/othergov/doe/lanl/lib-www/la-pubs/00326407.pdf>>. p 357-377
10. Sjoden, Glenn E., and Ce Yi. *Transport Simulation and Validation of a Synthetic Aperture SNM Detection System ("T-SADS")*. Quarterly Report Oct 2012. Print.
11. United States Department of Energy. ORIGEN code description. <http://www.ne.anl.gov/codes/origen/>

12. X-5 Monte Carlo Team. *MCNP - A General Monte Carlo N-Particle Transport Code*. Los Alamos National Laboratory, 24 Apr. 2003. Web. 9 May 2013.
13. Sjoden, Glenn E., and Ce Yi. *Transport Simulation and Validation of a Synthetic Aperture SNM Detection System ("T-SADS")*. Quarterly Report Jan 2012. Print.
14. Sjoden, Glenn E., Jessica Paul, and Michael Chin. *Mobile Pit Verification System Design*. N.p.: Department of State, 2012. 7-10. Print.
15. Price for Cadmium.
<http://www.sigmaaldrich.com/catalog/product/aldrich/265411?lang=en®ion=US>
16. Price for HDPE. http://www.eplastics.com/Plastic/HDPE_Sheet
17. Price for Hafnium. https://us.vwr.com/store/catalog/product.jsp?product_id=7484836
18. Price for Indium.
https://www.goodfellowusa.com/catalog/GFCat4J.php?ewd_token=JRLnjzfAVeoVOki9AEQbDgo8Xm2BKp&n=Nt1TTsU6ZSgnm5busdqr9JP7aWbIWt
19. Price for Tantalum.
http://www.goodfellow.com/catalogue/GFCat4J.php?ewd_token=X6ugosjM5bzdBONoCwzfG56J29wVFL&n=bEUltoBpOQwIInNFEo3NaCUQNAgsoV
20. Price for Foam. <http://www.amazon.com/Craft-Styrofoam-Foam-Sheets-Pack/dp/B0072IPXDW>